9. The Nucleation of Acicular Ferrite on Ti Based Inclusions

9.1 Introduction

The analysis of chapter 8 revealed the strong effect that chemical reaction between an inclusion and steel has upon the nucleation of ferrite at a ceramic/steel interface. These mechanisms, potent as they are, do not account for the nucleation of α_{acic} for several reasons:

(i) Silicon carbide is not readily formed in the weld pool as, generally, carbon levels are low and the activation barrier to formation of SiC is not easily overcome. Silica or silicates are much more likely at the oxygen levels present; the former has shown no tendency to act as a CAI to nucleate ferrite. Cobalt oxide also has not been reported as a constituent of weld metal inclusions and its high cost has prevented its widespread use in fluxes, although weld alloying with Co is being investigated for high toughness applications. The reaction with this ceramic is limited to the inclusion itself with little effect on the steel outside.

(ii) The mechanism of chemical activity promoting formation of α around SiC i.e. that of inclusion dissolution to release Si and C into solid solution. This results in enhanced Si levels around the inclusion compared with the bulk, but STEM analysis around nucleating inclusions in HSLA welds [65] failed to reveal any variation in substitutional alloying element concentration. The silicon levels recorded around inclusions are $\approx$ 0.4-0.5wt%, which are far below those needed for the effects seen with the SiC/steel diffusion bonds. EDS undertaken on α_{acic} during this project indicated that there was no variation in substitutional alloying elements concentrations either along or across an α_{acic} plate or extending over the α/γ interface. Further there was no difference between the α_{all}/γ and the levels recorded at the α_{acic}/γ interface, so that variation in [Si] is not responsible for the preferential nucleation of ferrite upon inclusions.

(iii) Nucleation of α_{acic} has often been associated with inclusions rich in Ti also with Al and Mn. Any dissolution of these oxides would release Ti into solid solution, which would locally increase the hardenability of the steel and retard nucleation of ferrite.

The body of evidence (section 6.3.3.2) for nucleation of α_{acic} on titanium oxides merits a closer examination of these inclusion phases and their relationship to the γ-α transformation. Some clue may be gained from the preceding chapter where both chemical reactions resulted in a change in the carbon level in the steel locally, albeit an increase. Indeed the local increase in [Cr] and [C] at the interface is sufficient to precipitate chromium carbides in both cases. Therefore, the studies of chapter 8 were extended to include those inclusion phases often associated with manual metal arc (MMA) and submerged arc (SA) weld metal for [O] levels around 200-300ppm, namely TiO, TiO_2, TiN, TiC, TiB_2, Al_2O_3, $Al_2Si_2O_7$, MnO and MnO_2.

9.2 Experimental

The same high hardenability steel 4857 (Fe-4.08wt% Cr-0.31wt% C) was used for these experiments as for those in chapter 8. In addition a 3.0 Mn-2.04 Si-0.22 C (wt%) steel (4862), unusable for the silicon studies was used with TiO_2. This was of similar composition to the weld metal PJ304 used in deducing phase transformation theory for α_{acic}. The steel was prepared as 10mm lengths as in chapter 8 and the 'composite' specimen set up in the same way. The applied pressures used were 12.5MPa and less, well below the yield stress of the steel, although yielding at the asperities occurred causing the inclusion to be embedded into the steel. This probably approximates well to the stress state around an inclusion in a cooling weld and helped to generate a more intimate interface to study chemical effects, lattice matching and stress transfer. The heat treatments are listed in Table IX.1.

9.3 Aluminium Based Ceramics

Welding Institute research [246] has highlighted the possibility of α_{acic} nucleation on alumina or alumino-silicates, although not all the changes introduced by the flux variation were taken into account. To test their nucleation behaviour, runs were carried out using Al_2O_3 and $Al_2Si_2O_7$ as ceramic interlayers, the composites being reaustenitised at 900°C for 10mins before isothermal treatment at 505°C for times between 60 and 900 seconds.

1. Alumina

The interface regions for 4857/Al_2O_3 are shown in fig. 9.1 and indicate that no ferrite nucleation occurred at the ceramic/steel interface. Microanalysis by EDS showed no change in substitutional alloying element concentration up to the ceramic, nor was there any significant change in hardness over the same region. This phase therefore exhibits no chemical activity and is merely acting as an inert surface which is insufficient to cause nucleation in this regime. The planar disregistry[1] is ≈ 16.0% [258] and so lattice matching is poor; however thermal strains may also be present through differential thermal expansivities.

2. Alumino-silicate

Unlike Al_2O_3, treatment of 4857/$Al_2Si_2O_7$ couples at 505°C for 60 and 900s after reaustenitisation at 900°C for 10mins caused the formation of a thin ferrite film along the steel/ceramic interface. After 60s at 505°C a continuous layer 4-6μm thick developed at the ceramic/steel interface, whereas the bulk of the steel was martensitic. The ferritic layer developed further into the grain along prior γ grain boundaries, doubtless due to faster growth and diffusion along these defects. In some cases, flow of metal took place around particles of the ceramic powder and the entrapped steel is seen to have fully transformed to ferrite, fig. 9.2. When the

[1] If $[uvw]_n$ of the nucleating particle is parallel to $[UVW]_\alpha$ of ferrite, the planar disregistry is given by:

$$100 \times \frac{(\text{interatomic spacing along } [uvw]_n) - (\text{interatomic spacing along } [UVW]_\alpha)}{(\text{interatomic spacing along } [UVW]_\alpha)}$$

isothermal treatment time was extended to 900s then the ferrite layer formed is not as uniform in thickness along the interface, although this may be due to inhomogeneities in the original powder interlayer, which may not have been of uniform thickness. Along the majority of its length the interface is decorated by a layer of ferrite that has developed to a thickness of ≈ 4-6μm into the steel. At one end of the interlayer, however, there has been interpenetration of the ceramic and steel with the latter flowing round particles of the former, fig. 9.3. This has probably occurred by plastic flow of the steel where less constraint existed due to the lower density of the interlayer, as, at the end, the particles are less tightly packed. The result of this is the formation of a much greater thickness of ferrite in this region, up to 12-16 μm. Inspection of the ceramic indicates the greater formation of ferrite leads to a discolouration of the interlayer, which adopts a uniform dark grey appearance when associated with areas of high transformation. This is in contrast to the speckled light/dark grey appearance for the ceramic associated with regions where less transformation has taken place. This is not due to compaction or sintering during heating and loading as this would be constant along the whole of the interface; its association with the amount of transformation might be chemical in nature or the result of volume changes upon formation of α.

9.4 Manganese Based Ceramics

The most common Mn based ceramic encountered in steels is probably the sulphide MnS, but this phase has not been reported as nucleating α_{acic} in weldments. Indeed, Evans [101] reports a decrease in the nucleation behaviour of inclusions when coated with a Fe-Mn sulphide film. The Welding Institute [256] also found that increased sulphide contents did not lead to increased α_{acic} nucleation, hence it was decided not to study the sulphide phases but to limit the investigation to manganese oxides. The two oxides studied, Mn(II)O and Mn(IV)O_2, had free energies of formation of ≈ 400-500kJmol^{-1} at 298K, a range of values that had previously exhibited chemical activity. The presence of Mn as one of the major alloying elements in low alloy weld deposits gives rise to the frequent presence of Mn oxides and silicates in weld metal inclusions. The formation of aluminium manganese silicates in medium (<50% Al_2O_3) alumina fluxes has been linked to nucleation of α_{acic}. The determination of the role of these phases is thus important. In order to provide a comparison with the other oxide series studied a standard reaustenitising treatment of 10 mins at 900°C was adopted, followed by a series of times at 505°C. The applied load was maintained at 100kg giving an applied pressure of 12.5MPa, this was applied at the start of the reaustenitisation treatment and removed during the quench from the isothermal treatment temperature.

9.4.1 Manganese (II) Oxide

This interfaced well with the steel to give a reasonably sound bond, but remained as a pale green powder. Optical metallography of the interface after both 60 and 900 seconds at 505°C, fig.

9.4, reveals the absence of any ferrite at the ceramic/steel interface. In the interfacial region of the steel, there was no change in the substitutional alloying element content, which correlated with the lack of any strong variation in microhardness. This is therefore another example of a chemically inactive inclusion.

9.4.2 Manganese (IV) Oxide

This oxide, when pure, is a highly reactive entity and so its reaction with steel came as no surprise. The interface region for a specimen held at 505°C for 5 minutes after reaustenitisation at 900°C for 10 minutes, fig. 9.5, indicates the formation of a layer of ferrite at the steel/ceramic interface. The ferrite layer is uneven, being ≈ 5μm thick along most of the interface, but, in some regions, extending up to 15μm into the steel. The latter regions are associated with areas of greater steel/ceramic interpenetration. Ferrite growth is also enhanced along prior γ grain boundaries. There may be a densification of the original powder, but this was not investigated further and could have resulted from the specimen loading during bonding. Cracking of the prior γ grain boundaries adjacent to the ceramic interlayer was observed, but the reason for this is not clear. Separation of the ceramic and steel occurs very readily, interface bond strength being very weak with the bond being held together at points of steel/steel contact.

9.5 Titanium Based Inclusion Phases

These compounds appear to be very important to α_{acic} nucleation, various ones being favoured by North et al. [257] (TiN), Mori et al. [258] (TiO) and Dowling et al. [259] (TiO_x) and so they merit extensive investigation. Pure powders of TiO, Ti_2O_3, TiO_2, TiC, TiN and TiB_2 were obtained; the oxides have been reported as inclusion constituents, the nitride and carbide have low lattice disregistry with ferrite and the boride is sometimes added to high toughness fluxes.

9.5.1 The Oxides

Initially each interlayer was used between blocks of 4857 and heat treated for 60s at 505°C following reaustenitisation at 900°C for 10mins. This treatment is insufficient to cause grain boundary nucleation of ferritic phases at grain boundaries within the bulk of the steel, which was fully martensitic. This allowed comparison of the nucleation behaviour of the steel/ceramic interface with prior γ grain boundaries. The resulting interface regions are illustrated in fig. 9.6 for each oxide and indicate the formation of a layer of ferrite at the steel/TiO_2 interface up to 10μm thick. The ferrite layer was observed to be of uniform thickness along the interface, showing no preference for any particular grain. These are of varying orientation and so a variety of lattice matchings should result along the interface, the absence of any preference indicating that lattice matching is not important. Growth into the steel was again seen to be accelerated along the prior γ grain boundaries. The shape of these grains of ferrite and their preference for grain boundaries suggest that they are diffusional in origin and hence are not bainite as the TTT diagram would indicate, nor are they α_{acic} plates. The corresponding interfaces for TiO and

Ti_2O_3 are devoid of ferrite, so that, under these conditions, they exhibit no nucleation behaviour, or one that is much less potent than that operating in the case of TiO_2. The same load (100kg) was applied for these tests and so the stress state experienced at the interface is the same indicating that this is not influencing the behaviour. Lattice mismatch between TiO and ferrite is much less than for Ti_2O_3 and TiO_2 and it is unlikely that this is a major factor in the nucleation of α at inclusion/steel interfaces.

9.5.2 Development of Ferrite at Steel/TiO_2 Interfaces

The steel/TiO_2 interface was further investigated to try to establish the effects of austenitising time, temperature and isothermal treatment on the ferrite layer. The various heat treatments are listed in Table IX.2.

9.5.2.1 Austenitising Treatment

Extension of the reaustenitisation treatment, either time (2-10 minutes) or temperature (1000-1200°C), causes an increase in the thickness of ferrite at the interface, fig. 9.7. However, increased reaustenitisation treatment also causes the quench time to increase, e.g. increased reaustenitisation time from 2 to 10 minutes caused the quench time to increase from 60 to 140s. The increased ferrite thickness may arise from processes active during the quench to the isothermal temperature or during the reaustenitisation. It is not possible to separate these two effects without greater control over the quench rate.

The resulting layer of ferrite at the steel/TiO_2 interface is seen to be composed of two layers, fig. 9.8, parallel to the original steel/TiO_2 interface. The layer adjacent to TiO_2 exhibits a very uniform thickness along the interface and its variation with isothermal holding time is small. However, the thickness of this layer increases with increases in both reaustenitising time and temperature.

In contrast, the second layer varies considerably with isothermal holding time and the majority of the ferrite thickening is associated with this layer. The two layers can now be associated with the two stages of the heat treatment; the one adjacent to TiO_2 forms during reaustenitisation and/or the quench and the second represents formation of ferrite during isothermal holding. It is the latter layer that develops preferentially along the prior γ grain boundaries.

The ferrite thicknesses observed in figs 9.6-9.9 and listed in Table IX.2 illustrate several trends:

(i) The thickness of ferrite increases with increased holding at the isothermal temperature, due to diffusional growth of ferrite.

(ii) Increased austenitising time and temperature, or their effects on subsequent cooling, cause increased ferrite formation.

(iii) There is negligible effect of pressure, in the range 0-12.5 MPa, on the thickness of ferrite formed.

These indicate the nucleation and growth of allotriomorphic ferrite during heat treatment at the steel/TiO_2 interface.

9.5.3 Titanium Nitride

The effect of lattice matching is further revealed by the use of TiN as an interlayer, which has a cubic lattice, a=4.064Å, enabling it to give a cube-on-cube orientation with γ and α. In fact O, C and N are interchangeable on a general TiX lattice and so similar effects viz surface effects are expected for all three. After the standard treatment of 60s at 505°C, the interface between 4857 and TiN - like that between 4857 and TiO - showed no evidence of ferrite formation, fig. 9.10. It can therefore be construed that the effect of lattice matching is a weak mechanism acting in the solid state nucleation of ferrite, although it may be effective in liquid- solid transformations. TiN had been proposed as being responsible for enhanced α_{acic} nucleation in Ti-B containing fluxes as it soaks up N to retain boron in solid solution, where the latter can segregate to γ grain boundaries and inhibit the nucleation of allotriomorphic α. The possibility exists that remanent TiB_2 from the flux still present in the weld metal may nucleate α_{acic} in these welds. Under the same conditions, however, no ferrite formed at the 4857/TiB_2 interface, a similar result occurring with both pure Ti sheet and wire (0.5μm diameter), fig. 9.11.

The results from this Ti-based series indicates that TiO_2 is a potent nucleation site, but that the other compounds studied (and pure Ti) are not effective. This leads to the conclusion that some chemical effect particular to the TiO_2 lattice is responsible as the same area and stress was used for all runs and the lattice matching of the TiX series is superior.

EDS examination of the interface region was used to determine to what extent any variation in substitutional alloying elements had been induced during the heat treatment. These traces, fig. 9.12, revealed that for both nucleating and non-nucleating inclusion phases there was no variation in the levels of substitutional alloying elements either in the ceramic or the steel. This is not unexpected for the nucleant phases as any diffusion of Ti into the steel or Fe into the ceramic would locally increase hardenability and retard ferrite formation. The absence of any substitutional element effects in the non-nucleant phases means that their behaviour arises because they are inert rather than because they react to release Ti or consume Fe.

Changes in elements with atomic numbers less than 13 (Al) cannot be detected easily using EDS (a windowless detector was not available and may not have been sensitive enough for the low levels involved here) and so variation of these elements may occur. Light elements also play a large role in nucleation, especially carbon and so any effect on these will be very potent and must be investigated.

It was therefore decided to study any carbon effects that may have occurred with respect to the ceramic. The formation of ferrite with TiO_2 means that studies of carbon in the adjacent steel for this couple will not reveal anything of interest as redistribution of carbon into γ from α will take place during growth of the ferritic phase. Therefore, laser microprobe mass analysis (LAMMS) was used to investigate the light elements in the ceramic phase. The theory of this

technique is detailed elsewhere [283], but is briefly covered here, fig. 9.13. The actual analyser used was a Cambridge Mass Spectrometry LIMA 2, in which the specimen was placed and the area of interest targetted using a He:Ne spotting laser. A laser pulse was then applied using the Q-switched Nd:YAG laser, which was frequency- doubled to give either a maximum pulse energy of 150mJ and 6-7ns pulse-length (wavelength=532nm), or frequency-quadrupled to an energy of 80mj, pulse length 4-5ns and wavelength 266nm. These result in a power density of 10^7-10^{11}Wcm^{-2} in the diffraction limited beam at the specimen. The application of this intense pulse over an area of ≈ 1μm in diameter causes evaporation of this small area of surface, down to a depth of ≈ 0.3μm. In addition the vaporised material is ionised and the resulting microplasma is accelerated through 3kV and the mass-to-charge ratio of the (positive) ions extracted from the plasma measured in a time-of-flight mass-spectrometer. The data from the spectrometer are then processed to effect the chemical analysis. This process analyses all elements including those, such as carbon and oxygen, outside the range of EDS. The technique is still relatively new and so is not fully quantified, one of the major problems being pulse-to-pulse variation, which leads to differences in the yield of each shot; the yield of each element also varies with its ionisation potential so that peaks cannot be directly compared. However, the technique is sensitive to small amounts of light elements and qualitative variations can be relatively easily detected, the detection limit for light elements being as low as 10ppm. Samples of TiO_2, TiO and Ti_2O_3 were analysed after heat treatment, bonded to 4857. As the composition of the steel was known, this was used as a standard to calibrate the spectra as the peak level for carbon could be compared with this known level (0.31wt%). To take account of shot-to-shot variability a series of ten shots was taken on the steel, well away from the interface area and so unaffected by events there. The mean value, corresponding to 0.31wt% C) of these shots is :

$$33163 \pm 14171$$

Spectra were then taken from the ceramic, often the yield varies dramatically between metals, ceramics and polymers, but in this case the overall yield was fairly similar, allowing a rough comparison of the peak heights.

The spectra obtained for TiO_2, TiO and Ti_2O_3 are shown in fig. 9.14 and indicate the presence of carbon in the first ceramic, but not in the latter two. Further investigation revealed that the carbon was not uniformly distributed, but separate light and dark regions existed in the interlayer, which corresponded to carbon-poor and carbon-rich peaks respectively, fig. 9.14a and b. The dark regions were scattered throughout the interlayer and were not concentrated at the interface, as might be expected and so could be carbon sinks in the original structure to which carbon migrated during the heat treatment. The use of lower beam energies results in less breakdown of the material in the plasma and forms some molecular ions, i.e. electrons are removed rather than bonds broken. When lower energy beams were used on the TiO_2 sample peaks were seen corresponding to TiO_2 and TiO, but no peak was observed for TiC, so that the formation of the carbide does not appear to have occurred. Instead the carbon is in solid solution

and comparison of the carbon peaks heights for the steel and ceramic gives a ratio of 10:1, indicating a carbon concentration of ≈ 0.03wt% in the ceramic. Low energy shots with TiO gave only peaks for TiO.

The action of the inclusion phases can now be deduced as being the removal of carbon into solid solution in the inclusion. This will locally decarburise the surrounding γ so reducing hardenability in the locality of the ceramic, promoting ferrite formation. The different behaviour of the oxides, therefore, must be due to variations in their lattice structures that allow carbon to dissolve in the TiO_2 lattice, but not in TiO, Ti_2O_3, Ti, TiC and TiN. The lack of any nucleation behaviour for TiC, fig. 9.15, compared with TiO_2 indicates that it is the removal of carbon from the steel that enhances ferrite formation rather than the formation of regions of TiC, which subsequently nucleate ferrite.

9.6 Titanium Based Inclusion Structures

9.6.1 Titanium Monoxide

TiO, like many transition metal low oxides, carbides and nitrides, adopts a cubic NaCl structure that is stable over a wide range of compositions TiO_x ($0.7 \leq x \leq 1.25$). Along with VO and NbO, TiO is notable for its non-stoichiometric nature with a structure containing large numbers of both metal and oxygen vacancies. The equiatomic oxide ($TiO_{1.0}$) contains ≈ 15% vacancies on both metal and oxygen lattices. As the concentration varies then the ratio of these vacancies changes with predominantly more O vacancies for $x<1.0$ (and the converse true for $x>1.0$) so that at $x=0.7$ the Ti lattice is almost defect free. The large number of defects involved means there must be some stabilising effect, which was found by Terauchi and Cohen [284], using diffuse-diffraction studies. The 'stoichiometric' composition was found to exhibit both vacancy-vacancy and vacancy-ion interactions stabilising the defect population, whereas only the latter interaction occurred for the sur-stoichiometric oxide $TiO_{1.25}$. The effective pair interactions in these structures are calculated at:

-105.42meV for $TiO_{1.01}$

-128.06meV for $TiO_{1.25}$

and are related to the Fermi level in these structures, falling just below it.

Various attempts have been made to model the electronic structure of non-stoichiometric TiO using approaches based on valence electron concentration (VEC) [285], electron-valence models [286], Bloch functions [287], virtual crystal approximations (VCA) [288,289] and linear combinations of atomic orbitals (LCAO) [290]. Full descriptions are beyond the scope of this work, but they are summarised in Table IX.3.

Calculations based on 27 atom clusters [291], e.g. $OTi_6O_{12}Ti_8$, representing the first three nearest neighbour sets indicates that oxygen vacancies lead to redistribution of wave functions into and increased electron density in the metal d states near the Fermi level. The metal-oxygen bonds have excess d occupancy as well as considerable 4s,p occupancy, forming diffuse electronic

states. The restriction of the cluster model to 3 shells neglects the vacancy-vacancy and vacancy-ion interactions noted above, which are dominated by 5th and 6th shell interactions. The redistribution of wave functions delocalises excess charge so that the charges for the components (inner shell) are:

	Vacancy cluster	Perfect cluster
Ti	+1.21e	+1.25e
O	-1.69e	-1.25e

Such large scale charge delocalisation, which is associated with a slight rearrangement of the 6-fold oxygen co-ordination shells, results in great stabilisation of the defect structure. It also indicates the high activation energy that is required to fill the vacancy by a heteroatom, such as carbon. In order to fill the vacancy, Ti-C bonding orbitals must be established acting across the former vacancy. However, in the vacant site, electron density across the vacancy is depleted, being redistributed into the metal d orbitals and remaining Ti-O bonds. Therefore, redistribution of electron density back into Ti-C orbitals will have to pass through a highly activated state, as the delocalisation stabilisation is removed.

The cluster model considers isolated vacancies and so is not able to model the vacancy interactions such as clustering and ordering, which occur at large concentrations of defects. These represent a step up in scale and have important effects on the structure and behaviour of the monoxide below ≈ 900°C. This corresponds to the temperature used in the nucleation study and merits further investigation.

TEM studies of various quenched specimens of TiO_x [292] have shown the presence of microdomains and ordered structures, whose nature varies with composition. No substructure is noted for the high temperature (1500°C) structure [illegible], but if annealed below 950°C numerous superlattice reflections are observed. These corresponded to equiaxed domains ≈ 3μm in diameter with a series of internal bands parallel to {110}of the cubic NaCl lattice. Careful indexing reveals a distortion of the cubic lattice into a monoclinic cell (a=5.855Å, b=9.340Å, c=4.142Å, γ=107°32'), which contains 12 Ti, 12 O and 16.7% vacancies. The defect structure that produces this cell can be visualised as one in which every third (110) plane of the high temperature cubic structure has half its oxygen and titanium sites missing alternately, fig. 9.16. This structure holds, at least, over the range $TiO_{0.9}$-$TiO_{1.1}$ with alternating variants forming to minimise ordering stresses.

The end-member of the TiO composition range ($TiO_{1.25}$) orders, at long times, below 900°C to a tetragonal cell (a=6.594Å, c=4.171Å), where the 22% vacant Ti sites are ordered on the body centring sites, fig. 9.17. Annealing intermediate compounds, e.g. $TiO_{1.19}$, for long periods at 700°C causes superlattice spots from both previous types of ordering to be observed with a microstructure consisting of domains with lamellae of TiO and $TiO_{1.25}$. The lamellae are ≈ 20Åthick and build up small domains ≈ 1μm in diameter. The interface planes of these lamellae have been indexed parallel to {120}of the cubic NaCl structure.

The various levels of stabilisation are necessary to enable the highly defective structure to exist and must, necessarily, mean that the oxide is less reactive than the vacancy concentration suggests.

9.6.2 Titanium Dioxide

The dioxide is also a non-stoichiometric oxide, which is oxygen deficient, exhibiting semi-conducting properties and can be generally represented as Ti_nO_{2n-1} ($\equiv TiO_{2-x}$). For small deviations from stoichiometry (large n) the low defect concentration is accommodated as a random solid solution. Decrease in n, however, results in the breakdown of the random solid solution as ordering into Magnéli phases [293]. These develop as a series of shear type phases, generally crystallographic shear (CS) phases. These CS phases are planar singularities that exist in substoichiometric, i.e. oxygen deficient, oxides of V^{4+}, V^{5+}, Nb^{5+}, Mo^{6+} and W^{6+} as well as Ti^{4+} ions, where the cations are octahedrally coordinated in oxide structures. An oxygen vacancy in this type of structure removes an oxygen from a shared apex or edge of the coordination octahedra, resulting in a high formal unscreened charge on the adjacent cations. These oxides also exhibit a high degree of metal-oxide orbital overlap and the stoichiometric changes are accommodated by a structural change on certain planes. Crystallographic shearing preserves the cation coordination, but results in the near elimination of a sheet of anion vacancies from the crystal, fig. 9.18. As the process is repeated throughout the crystal, a set of crystallographically defined structures is developed. These were first observed parallel to {121}of the cubic structure for low n phases, such as $Ti_{16}O_7$, but at higher n values {132}type CS phases are observed, up to $Ti_{36}O_{71}$. On approaching stoichiometry, the CS phases do not extend throughout the crystal, but are confined to domains. Their presence reduces the population of point defects randomly distributed and this is generally around 10^{-4}, calculated from the density and spacing of CS phases [294]. The latter quantity approaches an equilibrium value, so that the CS planes interact to align themselves into parallel groups with a long range interaction that results in an equilibrium spacing.

Introduction or elimination of CS planes is generally a slow, high activation energy process, but changes in composition are accommodated very readily by rotation of these planes. The planes remain largely planar, in preference to curving or kinking due to interfacial energy considerations and have been observed in TEM studies of $TiO_{1.90\text{-}1.98}$ [295].

The high temperature defect structure of the dioxide changes from one containing oxygen vacancies to one with interstitial Ti, a transition that can be interpreted by a shearing model.

Comparing the two oxide families $TiO_{1\pm x}$ and TiO_{2-x}, both exhibit ordering and large scale stabilisation of the defect populations at sizeable deviations from stoichiometry, which reduces the reactivity of these structures. At small deviations from stoichiometry, the defect population in TiO_2 is relatively random, consisting of point defects. TiO, however, still contains large numbers of defects and retains substantial amounts of defect interactions and stabilisation. The defects in the monoxide are, therefore, much less reactive than the corresponding species in the dioxide,

close to stoichiometry.

9.6.2.1 Energetics of Defects

Various models exist for the defect structure of TiO_{2-x} [296-300], which have been derived from measurements of x or σ (electrical conductivity) as a function of oxygen partial pressure P_{O_2}. Thermogravimetric techniques are generally used for determination of x and have been applied over the temperature range 800-1100°C [301]. This range is more applicable to these studies than other previous investigations, which concentrated on temperatures above 1000°C. Plots of log(x) vs. log P_{O_2} from the results of Marucco et al. [301], indicate linear regions, whose slopes vary from -1/6 (800°C) to -1/5 (1100°C). The change in slope can be attributed to a variation in the defect type so that, at high temperatures, interstitial titanium ($Ti^{4\cdot}$) exist, with an equilibrium given by:

$$Ti_{Ti}^{x}+2O_O^{x}=Ti_i^{4\cdot}+4e'+O_2(g) \quad .....(66)$$

$$K_{Ti}4.=[Ti_i^{4\cdot}][e']^4P_{O_2} \quad .....(67)$$

$$x=2[Ti_i^{4\cdot}] \ \alpha \ P_{O_2}{}^{-1/5} \quad .....(68)$$

The subscripts Ti and O refer to the Ti and O lattices respectively.

At lower temperatures, the dominant defect species is the doubly ionised oxygen vacancy, $V_O^{\cdot\cdot}$. For this species the relevant equations are:

$$O_O^{x}=V_O^{\cdot\cdot}+2e'+0.5O_2(g) \quad .....(69)$$

$$K_{V..}=[V_O^{\cdot\cdot}][e']^2[P_{O_2}]^{0.5} \quad .....(70)$$

$$x \ \alpha \ P_{O_2}{}^{-1/6} \quad .....(71)$$

Other regimes that exist are the CS phases and the singly ionised oxygen vacancies, $O^{\cdot}$, or impurity Fe^{3+} and Al^{3+}, which are affected by the doubly ionised oxygen vacancies.

The enthalpy of formation of these defects has been calculated from P_{O_2} measurements to give:

Defect	ΔH_f/kJmol^{-1}	
$Ti^{4\cdot}$	976.1 (10.1eV)	independent of x
$O^{2\cdot}$	441.7 (4.57eV)	independent of x
$O^{\cdot}$	372.1 (3.85eV)	x-dependent

The various enthalpies can be compared with the formation of a neutral defect and the sum of the necessary ionisation energies. Microcalorimetry measurements can be used to determine $\Delta H(O_2)$ associated with the non-stoichiometric TiO_2 oxygen system. At 1050°C, this value was found to be -977.0kJmol^{-1} [298], for the composition range $TiO_{1.995}$ to $TiO_{1.9999}$, which agrees well with Zador's -941.4kJmol^{-1} [302] derived from differentiation of $\Delta G(O_2)$, but splits the value of Forland, -878.6kJmol^{-1} [297], and Kofstad, -1096.2kJmol^{-1} [296]. From the constancy of these values, however, it can be deduced that the defects form a dilute solution at least between $TiO_{1.995}$ and $TiO_{1.9999}$, so that Henry's law can be applied to the randomly distributed defects. For the formation of doubly charged oxygen vacancies as in equation 69, the associated entropy change is:

$$\Delta S = S_{V_O^{\cdot\cdot}} + 0.5 S_{O_2} + 2 S_{e'} + S_{O_O^x} \quad .....(72)$$

and for an oxygen partial pressure of 1 atmosphere:

$$\Delta S(O_2) = -S\Delta S \quad .....(73)$$

Considering the various terms in eqn 72, a relationship of:

$$-2\left(\frac{\partial \Delta S}{\partial \ln x}\right)_T = 6R \quad .....(74)$$

The values for $V_O^{\cdot}$ and $Ti_i^{4\cdot}$ are 4R and 5R respectively.

Having determined the energetics of the defects it is necessary to ascertain, which of these defects, if any, carbon interacts with. Evidence of this comes from studies of oxidation, reaction with CO and ion implantation of titanium. The use of Auger, RHEED and energy loss spectroscopy [303] indicates the greater solubility of carbon in surface oxide layers rather than in bulk Ti with carbon occupying oxygen vacancies. This is shown by the carbon peaks in Auger and electron spectroscopy (ESCA) results on oxidation of Ti, where carbon, initially present as a carbide enters solution in TiO_2 as this layer forms. Ion implantation of steels with Ti and subsequent oxidation results in the formation of a surface layer rich in Ti, O and C, whose concentrations decrease further into the specimen.

The high formation energy of doubly charged oxygen vacancies would require some stabilisation to occur, some of this will be derived from entropy effects. It has also been proposed that carbon can stabilise oxygen vacancies, as large deviations of the O/Ti ratio from 2.0 can be tolerated if carbon diffuses into the vacancies created by oxygen migration [304]. Once carbon is removed, however, the rutile lattice is unable to maintain the large defect density and collapses. The results just mentioned were recorded during heating of Ti in dry oxygen and in the initial oxidation stages carbon is incorporated into the rutile surface as it forms. This illustrates that incorporation of carbon into the surface of rutile can readily occur to stabilise oxygen vacancies.

These results all generally refer to TiO_2 with a low degree of non-stoichiometry, when the defects can be assumed to be randomly distributed. No reports seem to have been made on the interaction of carbon with CS phases present at larger deviations from stoichiometry. The TiO_2 used in this study was close to stoichiometry and so the dissolution of carbon is due to the interaction of carbon with surface oxygen vacancies, which are randomly distributed point defects. The defect ordering that occurs with TiO to stabilise the high defect concentrations means that, although suitable sites may exist for carbon to enter ($O^{\cdot\cdot}$ vacancies), the activation energy for such a process is too high for this to take place. The microdomain structure would be disrupted on entry of carbon into the defects which would remove some defect stabilisation and oppose the entry of carbon. In TiO_2, the formation of CS phases probably has the same effect, in that the ordered structure resists disruption by carbon interaction. The CS phases also remove large numbers of vacancies to leave only a small residual population, with which carbon can interact.

9.7 Thermodynamics of Decarburisation by TiO_2

Assuming that TiO_2 causes decarburisation of the surrounding steel by accommodation in the oxygen vacancies, then the driving force for the process is two-fold.

(i) Removal of defects in TiO_2 releasing the excess free energy associated with them.

(ii) Lowering the free energy of austenite by the removal of carbon.

Point (ii) suggests that the decarburisation process becomes more favourable as the activity of carbon in γ increases during cooling and also that the effect will be larger in higher carbon steels.

EDS analysis indicates there is no change in substitutional alloying element content in either the ceramic or the steel and so equilibrium will only be achieved between the two phases with respect to carbon. Hence, the system is similar to a modified form of paraequilibrium and for carbon equilibrium between TiO_2 and γ, the chemical potentials for carbon in both phases must be equal:

$$\mu^{TiO_2}{}_1=\mu^{\gamma}{}_1 \qquad .....(75)$$

The subscript 1 refers to carbon.

The chemical potential of a component i in phase ϕ is given by:

$$\mu^{\phi}{}_i={}^{o}G^{\phi}{}_i+RTlna^{\phi}{}_i \qquad .....(76)$$

${}^{o}G^{\phi}{}_i$=solution free energy (or lattice stability) i.e. the free energy change to place i in phase ϕ from its standard state.

$a^{\phi}{}_i$=activity of i in ϕ.

Therefore, equation 75 becomes:

$${}^{o}G_1{}^{TiO_2} + RTln(a^{TiO_2}{}_1) = {}^{o}G_1{}^{\gamma} + RTln(a_1{}^{\gamma}) \qquad .....(77)$$

The previous discussion on the defect population in TiO_2 indicated that Henry's law applies to the oxygen vacancies and so should also apply to carbon filled vacancies, therefore:

$$a^{TiO_2}{}_1 \approx x^{TiO_2}{}_1 \qquad .....(78)$$

$x^{TiO_2}{}_1$=mole fraction of carbon in TiO_2

The activity coefficient of carbon in γ ($\gamma^{\gamma}{}_1$) can be estimated, in the low alloy regime, by Wagner interaction parameters:

$$ln(\gamma^{\gamma}{}_1)=\varepsilon_{11}x_1{}^{\gamma} + \varepsilon_{12}x_2{}^{\gamma} + \varepsilon_{13}x_3{}^{\gamma} + ... \qquad .....(79)$$

Subscripts 2, 3, etc. refer to the other alloying elements in steel, e.g. Mn, Si and Cr.

$x_i{}^{\gamma}$=mole fraction of i in γ.

Hence, $ln(a_1{}^{\gamma})$ can be replaced by:

$$ln(x_1{}^{\gamma}) + (\varepsilon_{11}x_1{}^{\gamma} + \varepsilon_{12}x_2{}^{\gamma} + \varepsilon_{13}x_3{}^{\gamma} + ...) \qquad .....(80)$$

The Wagner interaction parameters and ${}^{o}G_1{}^{\gamma}$ can be accurately estimated and so the right hand side of equation 77 can be calculated. The problem lies in ${}^{o}G_1{}^{TiO_2}$ for which no data is readily available. This energy term represents the transfer of C from its graphitic form into solution within the TiO_2 lattice, occupying oxygen vacancies. As the introduction of C into TiO_2

removes an oxygen vacancy, then this will release some of the energy of formation of that defect. In addition, there will be changes in the entropy terms for the random defect solution dependent upon the fraction of vacancies filled.

The nature of bonding has also changed with C now bonded to Ti in a tetragonal (c.f. a cubic lattice for Ti-C) compared to the C-C bonding in graphite. This change in bonding nature causes some charge stabilisation to delocalise the excess charge introduced by the vacant site. Therefore, the free energy of solution of C in TiO_2 cannot be approximated to the free energy of the vacant site, which it replaces. It is clear, however, that there is a sizeable driving force for carbon solution in TiO_2 and it is likely that the solution energy of C in TiO_2 is more negative than that of C in γ. On this premise it is possible to deduce a lower limit for the decarburisation of γ by TiO_2 and the subsequent increased driving force for ferrite formation. By equating the solution free energies of C in TiO_2 and γ, equation 77 becomes:

$$\ln(a^{TiO_2}{}_1) \approx \ln(x^{TiO_2}{}_1)=\ln(x^{\gamma}{}_1) + (\varepsilon_{11}x_1+\varepsilon_{12}x^{\gamma}{}_1+...) \quad .....(81)$$

The approach now adopted being to assume a value of $x_1{}^{TiO_2}$ based on the LIMA results (section 9.3.2) and calculate the value of $x^{\gamma}{}_1$ that satisfies equation 81. the initial value selected for $x^{\gamma}{}_1$ is the bulk composition and a Newton-Raphson iteration method is used to solve equation 81 for $x^{\gamma}{}_1$. The resulting value of $x^{\gamma}{}_1$ at the γ/TiO_2 interface after decarburisation is then used in the TTT prediction program [81], as used in the BSG model, to calculate the shifts in transformation behaviour induced by TiO_2.

Table IX.4 lists $x_1{}^{TiO_2}$, $x_1{}^{\gamma}$ after decarburisation and the change in $\Delta G^{\gamma-\alpha}$ (free energy for γ-α transformation at 505°C) c.f. bulk metal at various temperatures. Also listed are the incubation times for allotriomorphic ferrite formation at the ferrite nose, from which it can be seen that the experimental cooling curve will cross the diffusional C curve, if decarburisation takes place. The analysis is seen to be inaccurate and entropy effects mean that as $x_1{}^{TiO_2}$ decreases then greater decarburisation takes place. A limit of the number of vacancies and the amount of TiO_2 available for decarburisation needs to be incorporated. Hence, once decarburisation of the steel adjacent to TiO_2 has occurred at 900°C during reaustenitisation, allotriomorphic ferrite would be expected to form during cooling at the steel/TiO_2 interface, as was observed. The variation in ferrite thickness with time at 505°C then results from growth of the nucleated α into γ away from the steel/TiO_2 interface. This also explains why it was not possible to avoid allotriomorphic α formation and study the nucleation of bainite with this equipment. In order to do that either:

(i) The quench rate must be significantly increased by use of a smaller chamber and/or helium quenching directed at the interface, or:

(ii) Lower carbon, higher alloy steels must be used, as the effect is enhanced by high carbon levels. With lower carbon levels, the decarburisation process will take place less readily at higher temperatures and will be shifted to lower temperatures, where $a_1{}^{\gamma}$ increases. Higher alloy steels will be required to maintain hardenability.

Point (ii) illustrates the probable role of TiO_2 in nucleating α_{acic}, as lower carbon levels are experienced in welding situations, which would shift the nucleation behaviour down into the bainitic transformation regime.

If decarburisation occurs at too high a temperature then the possibility of intragranular nucleation of allotriomorphic ferrite exists, giving rise to ferrite islands. Additionally, if grain boundary allotriomorphic ferrite forms then carbon is partitioned into the remaining γ so raising the hardenability of these regions. Decarburisation around TiO_2 may then provide that extra driving force required to promote intragranular nucleation of bainite over nucleation at α/γ interfaces, resulting in an α_{acic} microstructure.

Slow cooling, as in high heat input processes, such as submerged arc (SA) welding, may allow sufficient time for redistribution of carbon in γ around TiO_2 particles. As the TiO_2 particles become saturated in carbon as the vacant sites are filled, diffusion of carbon in γ to level out composition gradients would remove the nucleation behaviour of the TiO_2 particles.

9.8 Further Nucleation Studies

The action of oxygen vacancies in TiO_2 in removing carbon from solid solution in γ would suggest that similar non- stoichiometric oxides could also be chemically active inclusions. The similarity between the oxides of vanadium and titanium has previously been mentioned and V_2O_5 is the vanadium equivalent of TiO_2, both structurally and chemically. Oxides of vanadium may also be present in weld deposits by dilution effects when welding HSLA steel baseplates. Therefore, samples of 4857 were interfaced to V_2O_5 and reaustenitised (in INTER) at 900°C for 10 minutes before quenching to isothermal holds at 505°C for 60, 300 and 900s. Specimens were also continuously cooled to room temperature from 900%sp C and isothermal holds at 550 and 450°C for 300s after reaustenitisation were also studied for comparison.

Fig. 9.19 shows the resulting ceramic/steel interface region for the heat treatments listed above. These indicate the formation of a thin layer of ferrite at the steel/V_2O_5 interface, which increases in thickness with holding time at 505°C, fig. 9.20. The layer is absent in the continuously cooled specimen, but increases to $\approx$ 6μm after 900s at 505°C. Similar thicknesses are observed after 300s holding at 450, 505 and 550°C, the ferrite being slightly thicker in the first case, probably due to the greater driving force for ferrite formation , once nucleated, at lower temperatures.

EDS again revealed no variation in substitutional alloying element concentration in the vicinity of the steel/ceramic interface, fig. 9.21. The LAMMS spectrum, fig. 9.22, gave a very low yield and revealed only V, O and V_2O_5 peaks. It is probable, with such a low yield, that carbon was not detected in the small sample area available.

It appears that V_2O_5 acts in a similar manner to TiO_2 by locally decarburising the adjacent steel, the carbon entering vacant lattice sites in the oxide structure. The thicknesses of ferrite obtained for steel/V_2O_5 interfaces are less than those for the corresponding steel/TiO_2 interfaces.

This may be due to the oxygen vacancies in V_2O_5 having a lower free energy and reactivity than those in TiO_2 and/or the resulting M-C interaction being more favourable for M=Ti than for M=V. The latter point is borne out in the precipitation processes in HSLA steels, where TiC exsolves in γ, but VC precipitates at th α/γ interface, at much lower temperatures, indicating a stronger Ti-C interaction than V-C.

The nucleation behaviour of Ti and (less potently) V oxides is also consistent with the observations (section 2.5.5.9), that the optimum V level for α_{acic} formation was dependent upon the Ti content present in the weld deposit. This can be seen to tie in with the provision of sufficient chemically active inclusions of the decarburisation type to nucleate α_{acic}.

Finally, runs were performed using Y_2O_3 and ZrO_2 coupled with 4857, Table IX.5. The interface regions of these specimens are shown in fig. 9.23 and indicate very little nucleation behaviour for either species, although some α may be present for $4857/Y_2O_3$.

These results also agree with the carbon-oxygen vacancy model, as the defect density (of oxygen vacancies) in ZrO_2 is low and that of Y_2O_3 is heavily stabilised so that both oxides are relatively unreactive.

9.9 Summary

The mechanism for inclusion nucleation of ferrite that would be compatible with the formation of α_{acic} in welds can be deduced as localised decarburisation of the steel in the vicinity of an inclusion. To remove carbon from the steel the inclusion must possess vacant lattice sites suitable for carbon occupancy and must interact favourably with carbon. The defect population must be sufficiently energetic to react, but not so high that ordering or CS phase formation occurs to stabilise it.

These conditions are met by high valence transition metal oxides, which have a random array of oxygen vacancies, which can accommodate carbon. The variable valency of the metal allows it to stabilise the initial defect somewhat, but also to interact with carbon establishing M-C bonding orbitals.

The formation of ferrite with $Al_2Si_2O_7$ is probably associated with charge centres or dangling bonds introduced into the SiO_2 network by Al. The possibility also exists of oxygen vacancies in the silicate network of a suitable size and charge to accommodate carbon. This is consistent with the nucleation of α_{acic} on manganese-alumino-silicates and galaxite (Al_2O_3MnO) [305].

These *chemically active inclusions* are the most potent nucleation sites, but in their absence, or the absence of carbon, the other (weaker) proposed mechanisms may come into prominence.

Table IX.1. Heat treatment details for Al, Mn and Ti based ceramics.

Steel	Ceramic	Reaustenisation temperature/°C	time/s	Quench time/s	Isothermal temperature/°C	time/s
4857	Al_2O_3	900	600	55	505	60
4857	Al_2O_3	900	600	180	450	180
4857	$Al_2Si_2O_7$	900	600	110	502	60
4857	$Al_2Si_2O_7$	900	600	118	503	900
4857	MnO	900	600	120	503	60
4857	MnO	900	600	110	503	900
4857	MnO_2	900	600	105	503	300

Steel	Ceramic	Reaustenitisation temperature/°C	time/s	Quench time/s	Isothermal temperature/°C	time/s
4862	TiO_2	1200	600	-	417	30
4862	TiO_2	1000	600	-	416	30
4857	TiO_2	900	600	132	550	30
4857	TiO_2	900	120	60	550	30
4857	TiO_2	900	60	quenched to room temperature		
4857	TiO_2	900	60	75	505	60
4857	Ti(wire)	900	600	112	505	60
4857	TiB_2	900	600	110	505	60
4857	TiN	900	600	104	505	60
4857	TiC	900	600	105	505	60

Table IX.2. Extra 4857/TiO_2 heat treatments after reaustenitisation for 10 minutes at 900°C.

T_{iso}/°C	t_{iso}/s	t_q/s	P/MPa	α width/μm	2nd layer/μm
550	30	132	0	4.5-5.0	2.3
550	30	83	12.5	3.8-4.5	1.5
450	90	190	0	4.5-6.0	-
450	90	155	12.5	3.8-5.2	-
505	60	75	0	6.0	-
505	60	112	12.5	7.5	-

P=bonding pressure, t_q=quench time to isothermal temperature

Table IX.3. Models for TiO defect structure.

Model	Basis	Comments
Valence Electron Concentration	Non-stoichiometry does not affect distribution of density of states, only occupation	Lowering of Fermi energy stabilises defect structure. Suggests vacancies stabilise *any* compound.
Electron-valence	Vacancies form new local levels near the Fermi energy	Essentially qualitative
Virtual Crystal Approximation	Treat vacancies as a potential dependent on their concentration	Quantitative, but poor correlation with data as limited to small density of states
Bloch wave formalism	Tight binding approach	Quantitative, but Fermi energy increases with density of states
LCAO	Quantum mechanical	Semi-empirical, good agreement

Table IX.4. Carbon mole fraction in TiO_2 (x_1^{TiO2}) and austenite (x_1^{γ}) and ferrite nose (T_i, t_i).

$x_1^{TiO_2}$	T/°C	x_1^{γ}	$\Delta G^{\gamma-\alpha}$/Jmol^{-1}	T_i/°C	t_i/s
0.01	900	0.0011	-95	720	1.7
0.01	800	0.0007	-98	740	1.7
0.01	700	0.0004	-100	740	1.8
0.01	600	0.0003	-104	720	1.8
0.01	500	0.0001	-106	760	1.6
0.02	900	0.0023	-89	720	2.9
0.02	800	0.0016	-92	720	2.4
0.02	700	0.0010	-102	720	1.8
0.02	600	0.0006	-99	740	1.8
0.02	500	0.0003	-104	720	1.8

Table IX.5. Heat treatments for 4857/Y_2O_3 and 4857/ZrO_2 after reaustenitisation for 10 minutes at 900°C.

Ceramic	T_{iso}/°C	t_{iso}/s
Y_2O_3	503	60
Y_2O_3	503	300
Y_2O_3	502	900
ZrO_2	504	60
ZrO_2	504	900
ZrO_2	548	300
ZrO_2	450	300

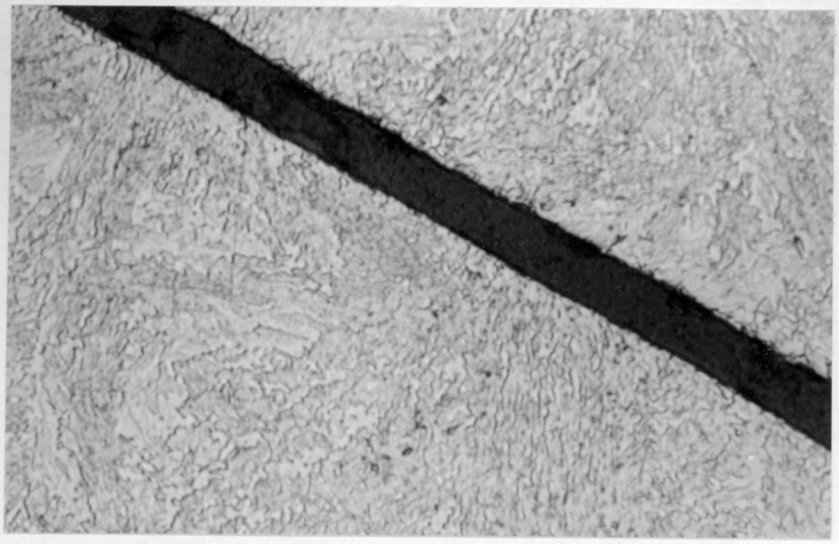

Figure 9.1. Interface region for 4857/Al_2O_3 (900°C 10mins - 505°C 60s).

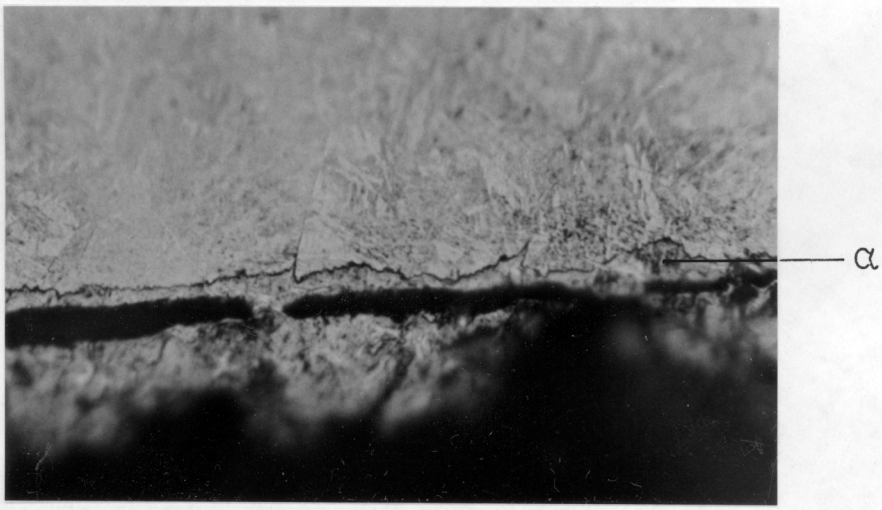

Figure 9.2. Interface region for 4857/$Al_2Si_2O_7$ (900°C 10mins - 505°C 60s).

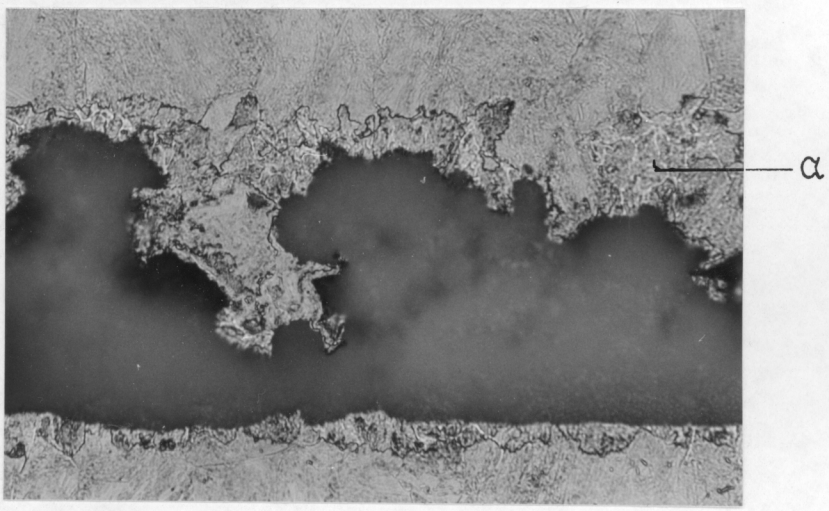

Figure 9.3. Interface region for 4857/$Al_2Si_2O_7$ (900°C 10mins - 505°C 900s).

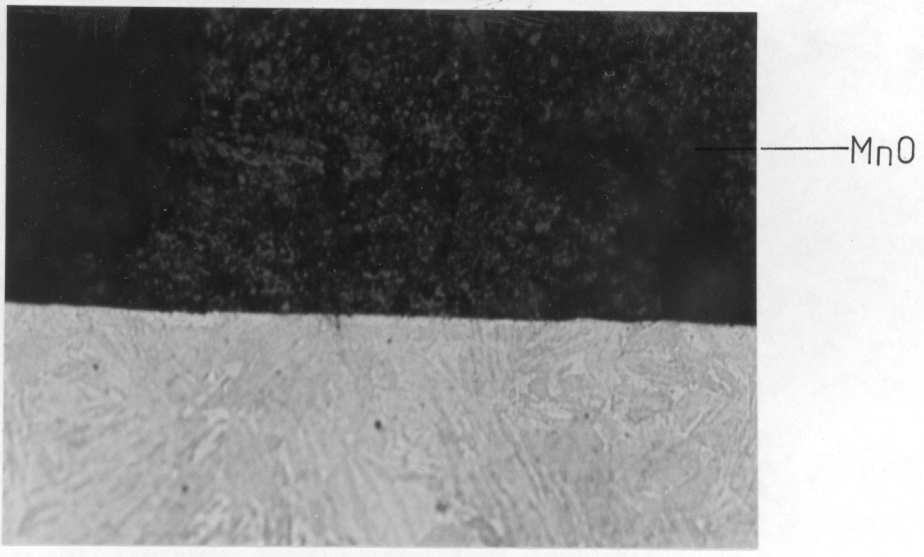

20μm

Figure 9.4. Interface region for 4857/MnO (900°C 10mins - 505°C 60s).

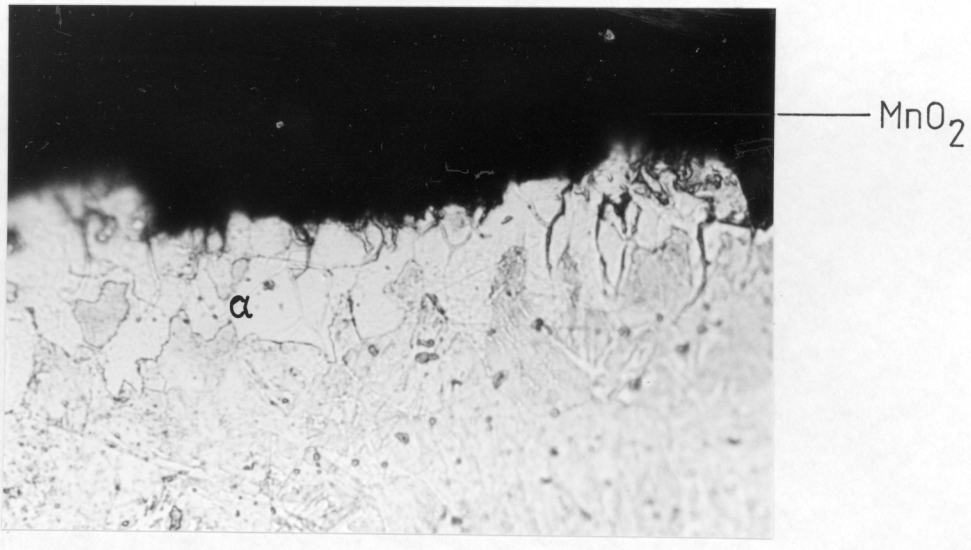

10μm

Figure 9.5. Interface region for 4857/MnO_2 (900°C 10mins - 505°C 300s).

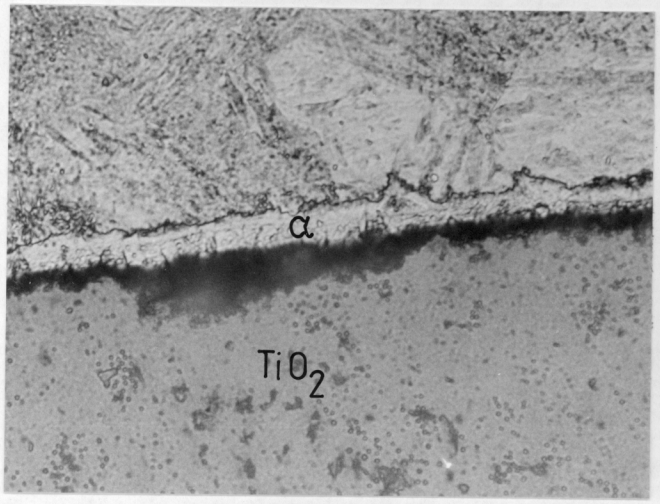

15μm

9.6(a) 4856/TiO_2

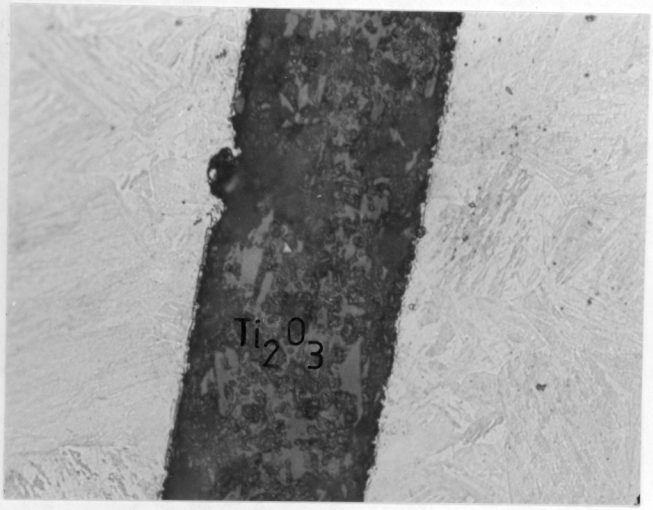

18 μm

9.7(b) 4857/Ti_2O_3

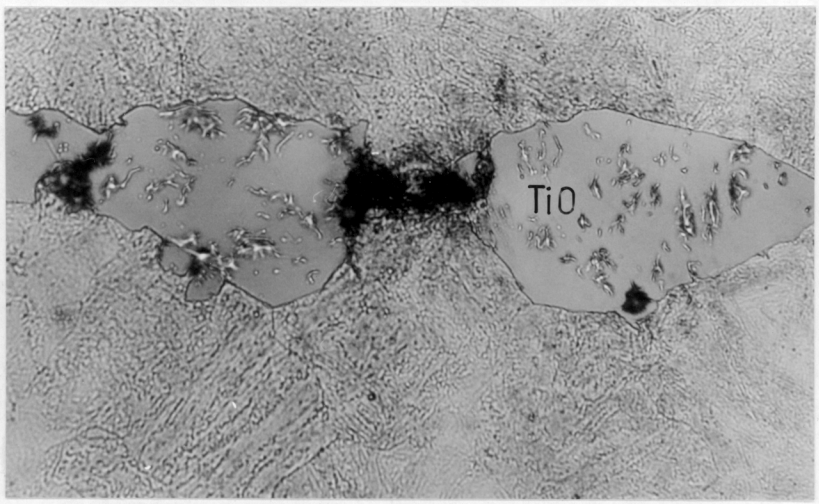

15μm

9.6(c) 4857/TiO

Figure 9.6. Steel/titanium oxide interfaces, 900°C/10 mins - 505°C/60s.

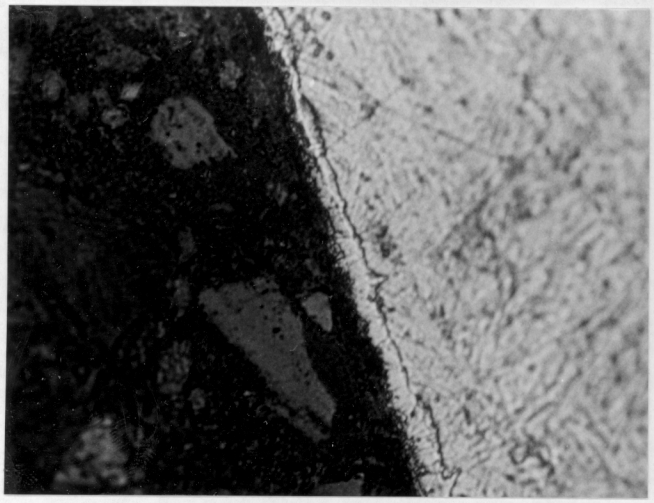

(a) 10μm

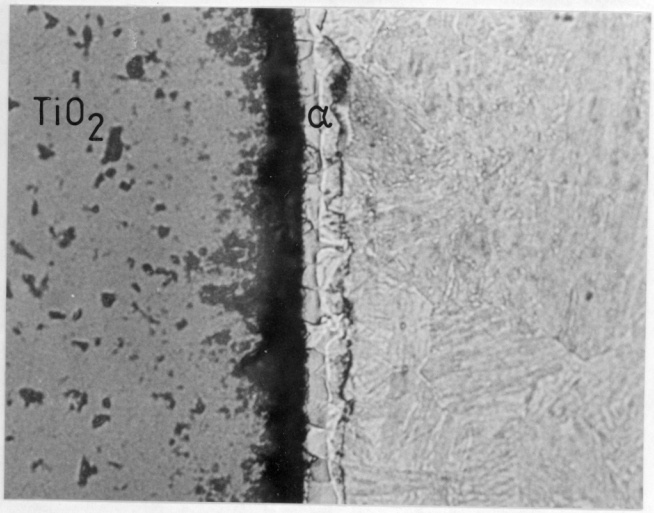

(b) 15μm

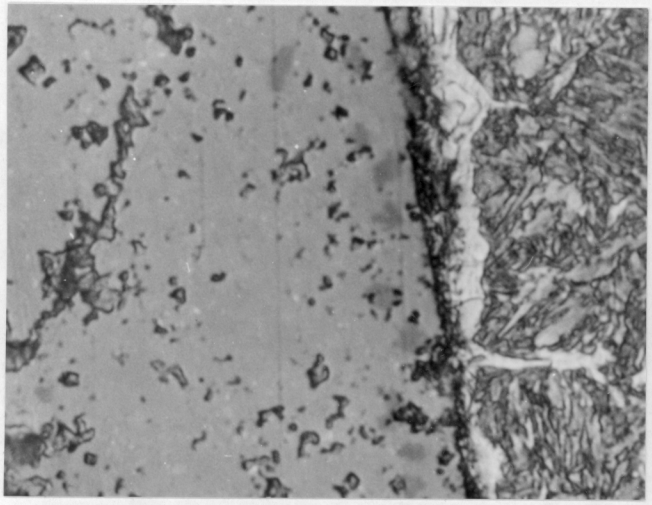

(c) 7.5μm

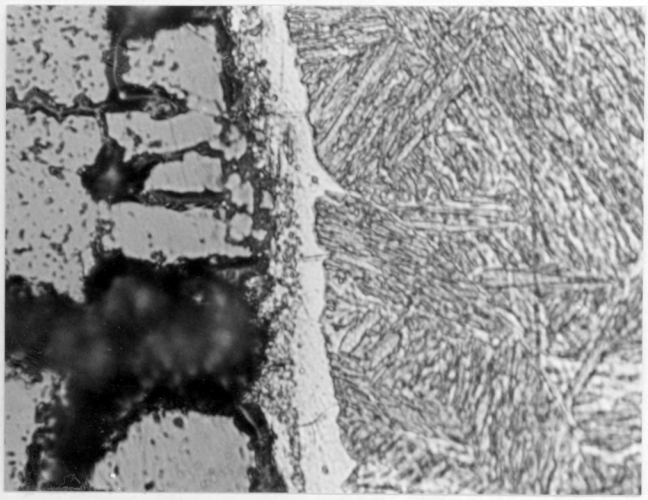

(d) 15μm

Figure 9.7. Effect of reaustenitisation treatment on ferrite formation at steel/TiO_2 interface, (a) 4857, 900°C/2 mins-550°C/30s, (b) 4857, 900°C/10 mins-550°C/30s, (c) 4862, 1000°C/10 mins-416°C/60s, (d) 4862, 1200°C/10 mins-400°C/60s.

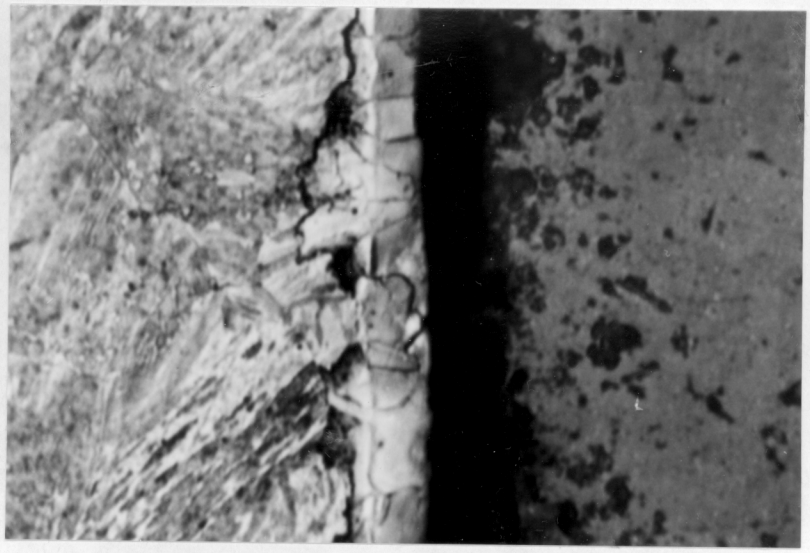

7μm

Figure 9.8. Duplex ferrite layer at steel/TiO_2 interface.

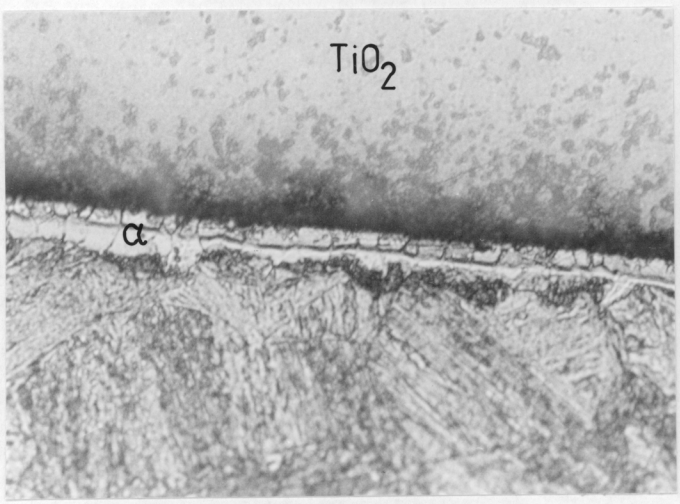

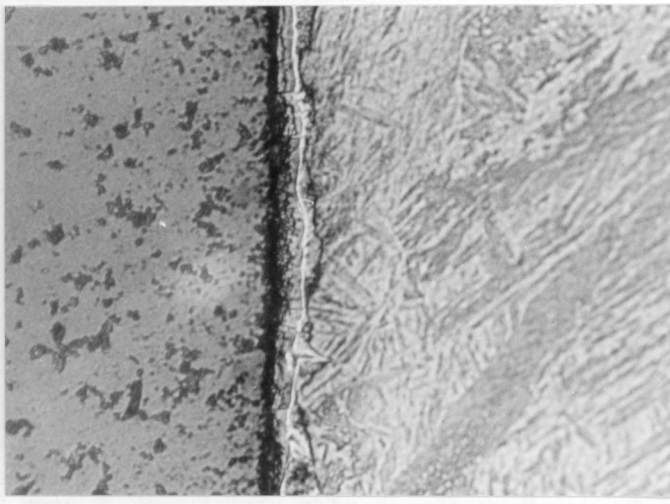

12μm. 0MPa. 12μm. 12.5MPa.

Figure 9.9. Interface regions for 4857/TiO_2 couples under varying load. 900°C/10 mins-450°C/90s.

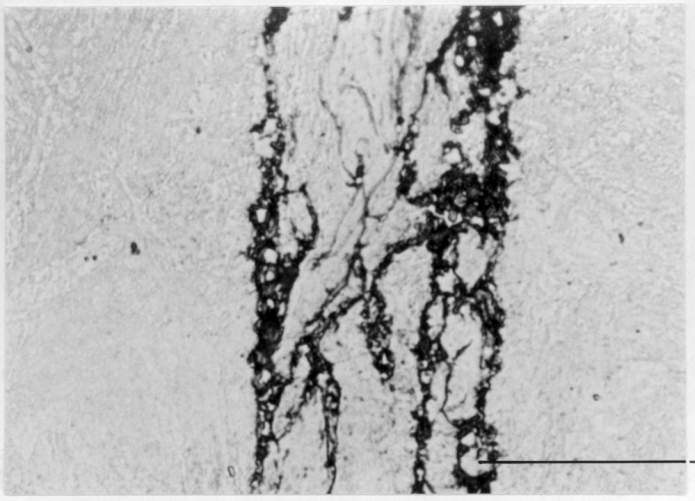

12μm

Figure 9.10. 4857/TiN interface region, 900°C/10 mins 503°C/60s.

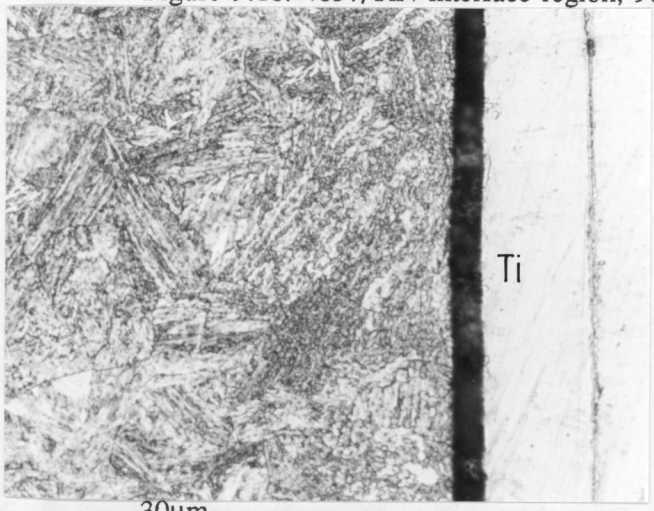

30μm

9.11(a) 4857/Ti wire

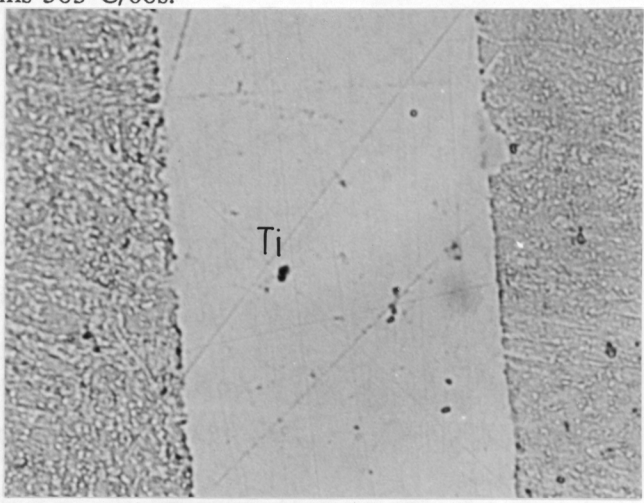

12μm

9.11(b) 4857/Ti sheet

30μm

9.11(c) 4857/TiB_2

Figure 9.11. 4857/Ti and 4857/TiB_2 interfaces after reaustenitisation at 900°C for 10 minutes then 60s at 505°C.

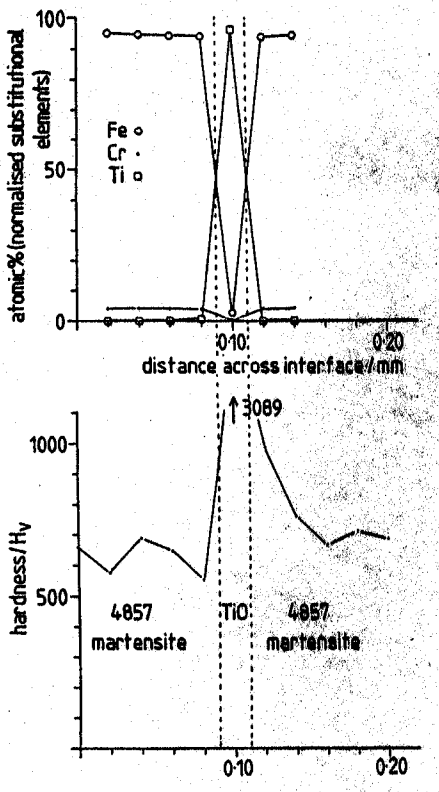

(a) 4857/TiO

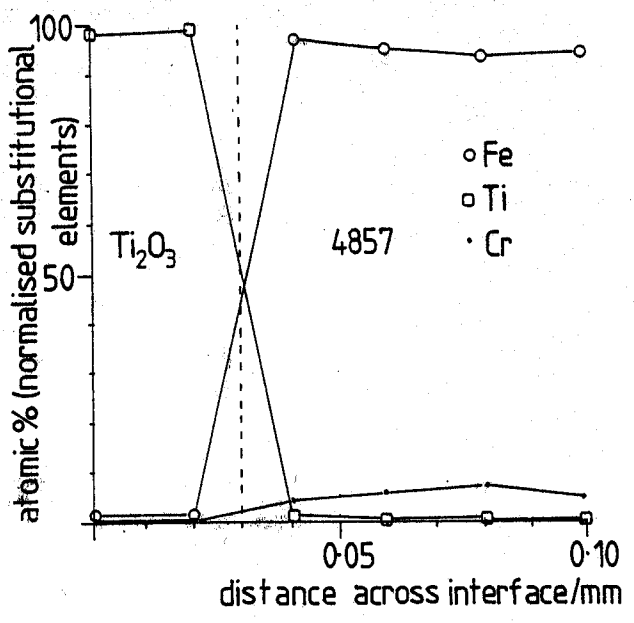

(b) 4857/Ti_2O_3

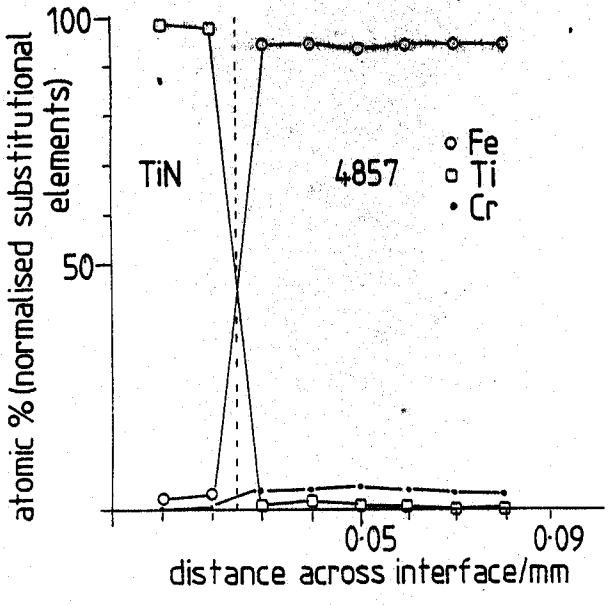

(c) 4857/TiN

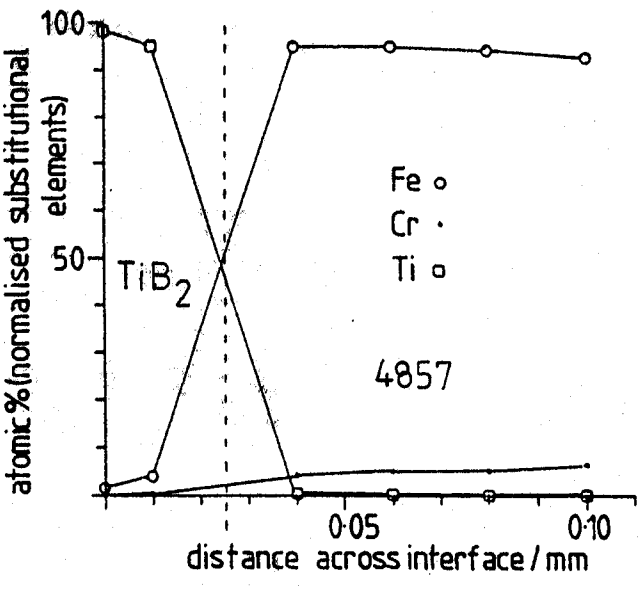

(d) 4857/TiB_2

Figure 9.12. EDS traces across steel/ceramic interfaces.

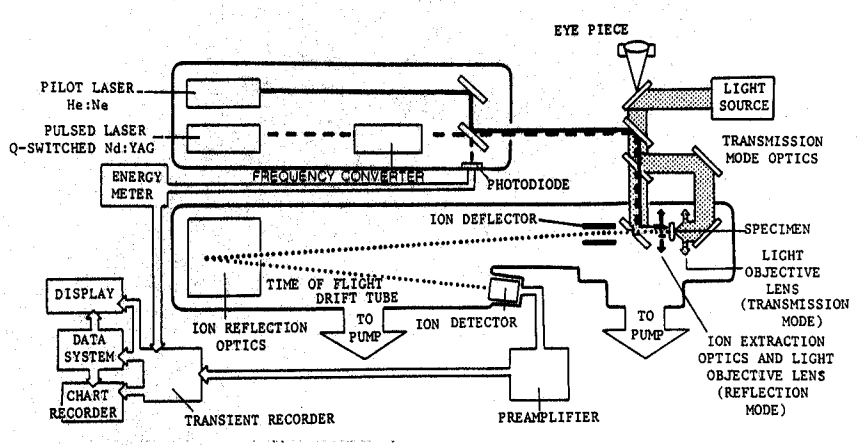

Figure 9.13. Schematic diagram of LAMMS apparatus.

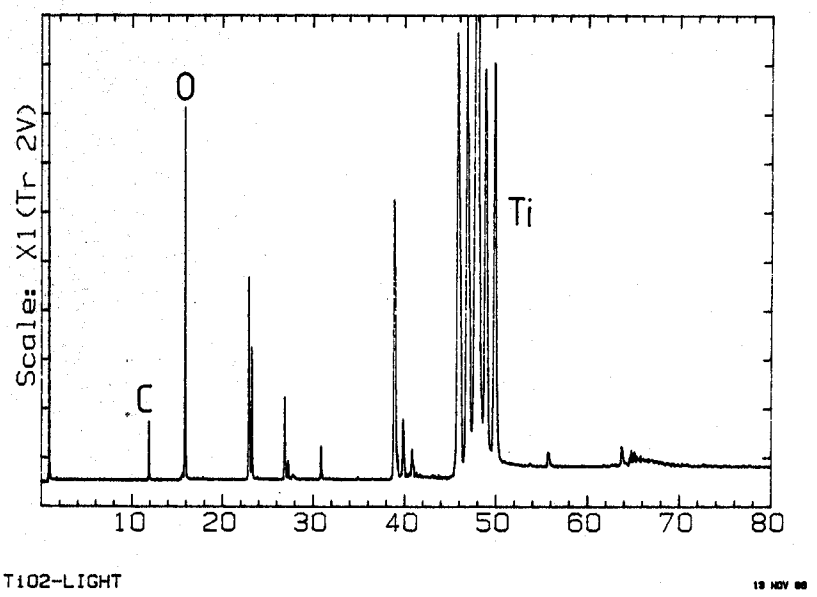

9.14(a).

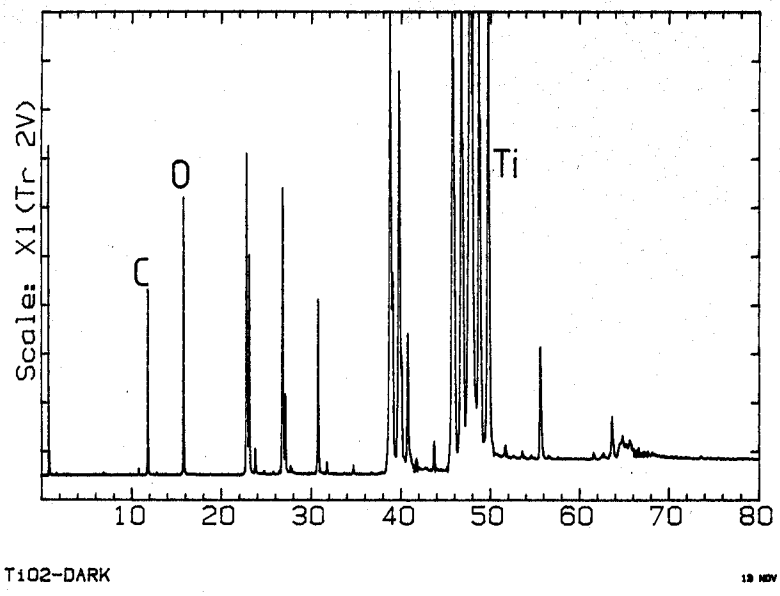

9.14(b).

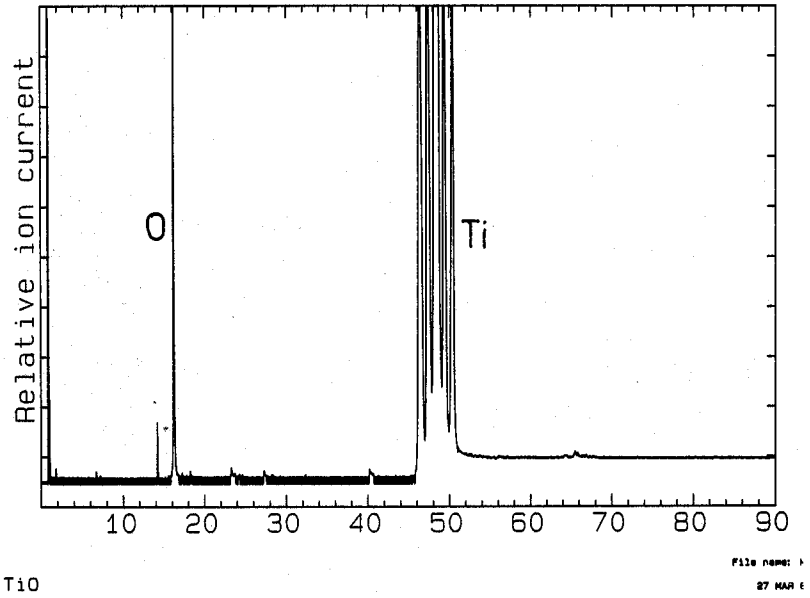

9.14(c).

Figure 9.14. LAMMS spectra for titanium oxides after heat treatment.

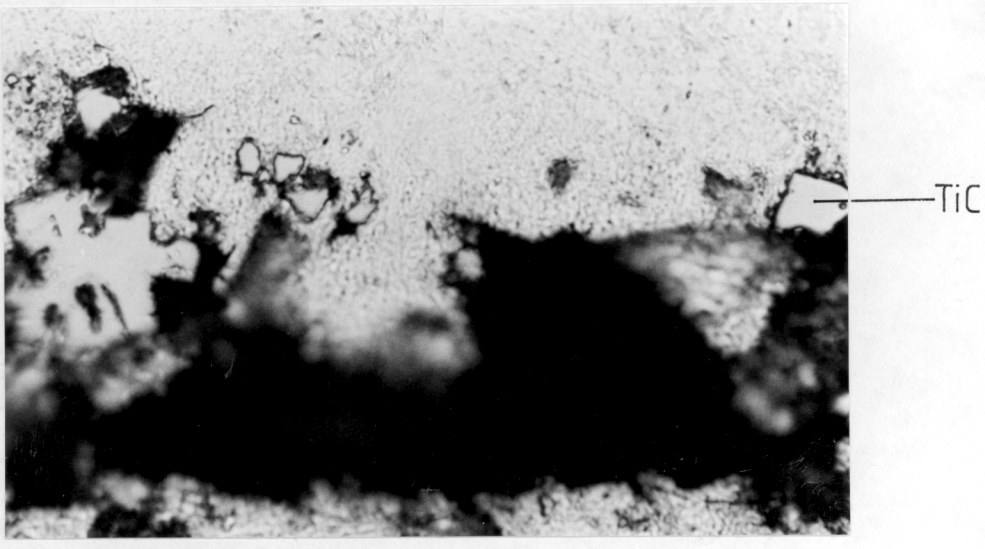

15μm

Figure 9.15. Absence of ferrite at 4857/TiC interface, 900°C 10 mins-503°C 60s.

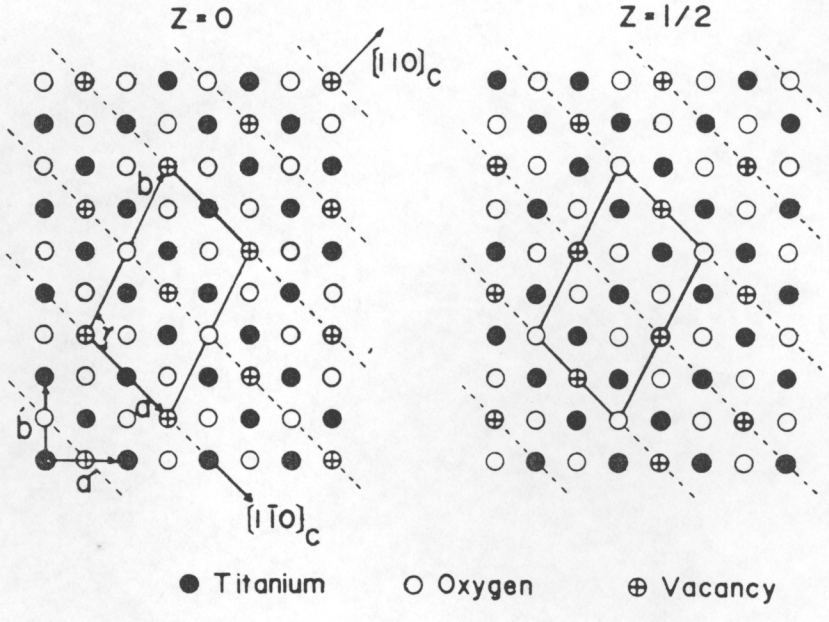

Figure 9.16. Ordered structure for $TiO_{0.9}$-$TiO_{1.1}$ [292].

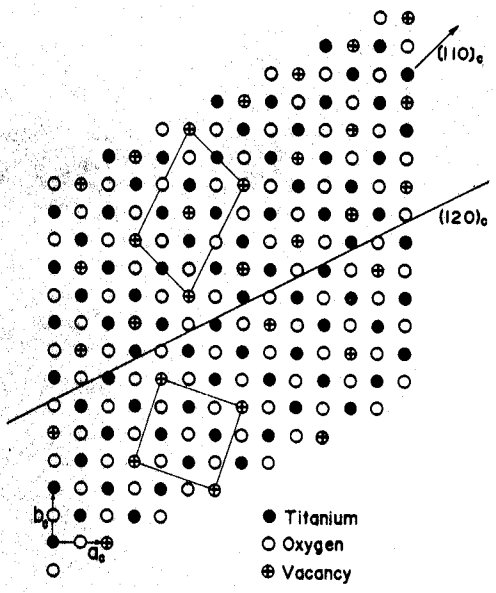

Figure 9.17. Ordered structure for $TiO_{1.25}$ [292].

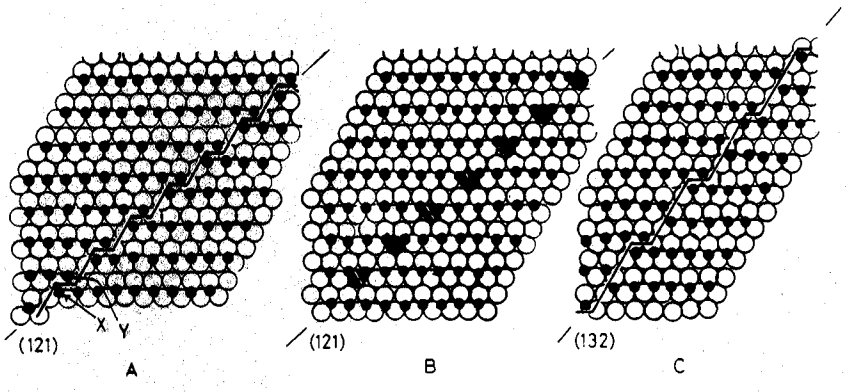

Figure 9.18. Formation of CS phases in non-stoichiometric titanium dioxide.

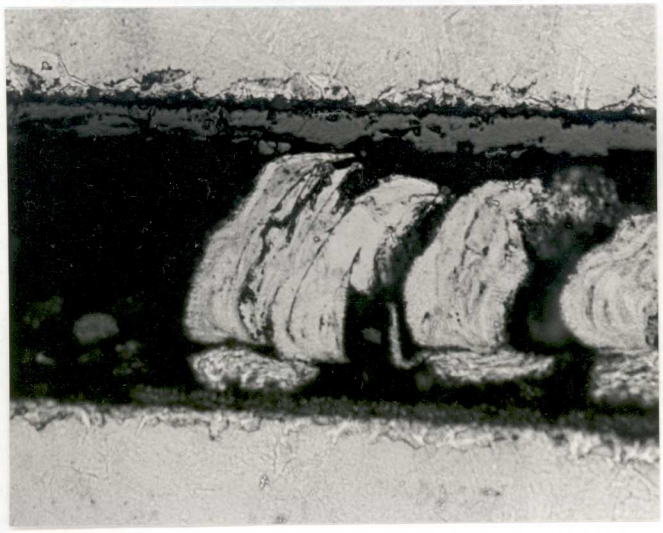

(a) 12μm

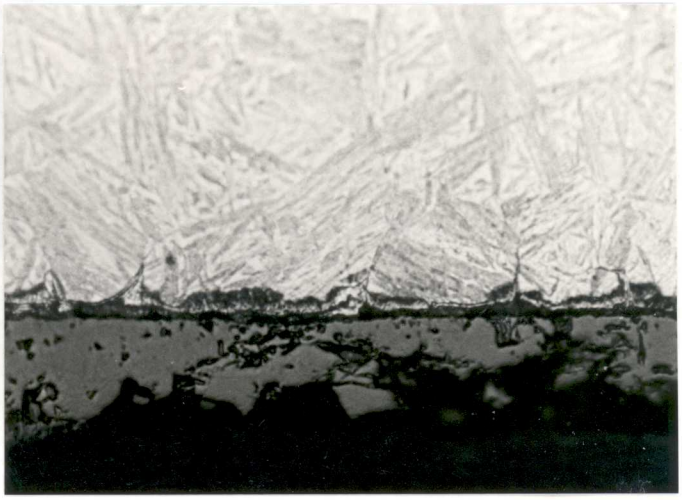

(b) 12μm

(c) 15μm

(d) 15μm

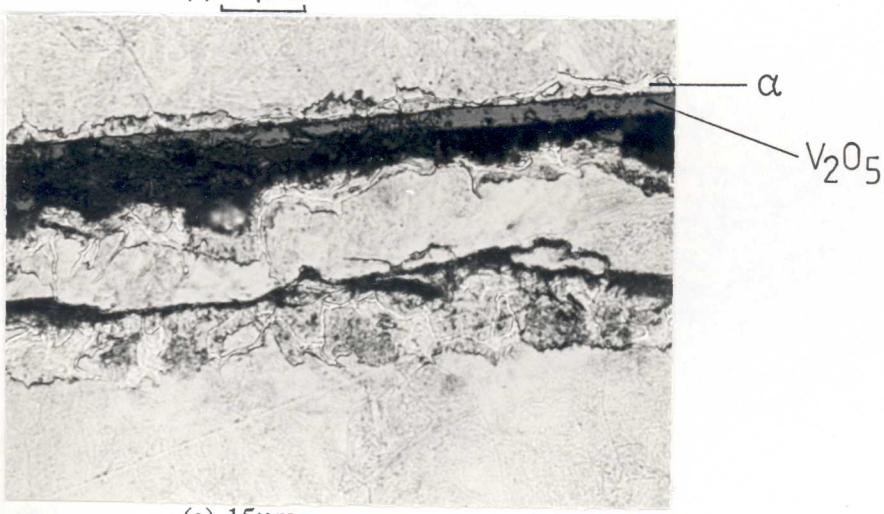

(e) 15μm

Figure 9.19. 4857/V_2O_5 interfaces reaustenitised at 900°C for 10 mins then (a) held at 505°C for 60s, (b) 505°C/300s, (c) 505°C/900s, (d) 450°C/300s, (e) 550°C/300s.

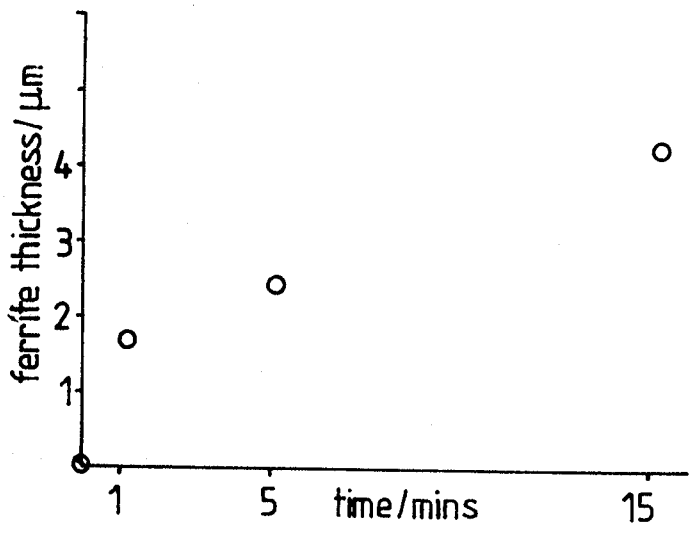

Figure 9.20. Variation of ferrite thickness at 4857/V_2O_5 interfaces with holding time at 505°C.

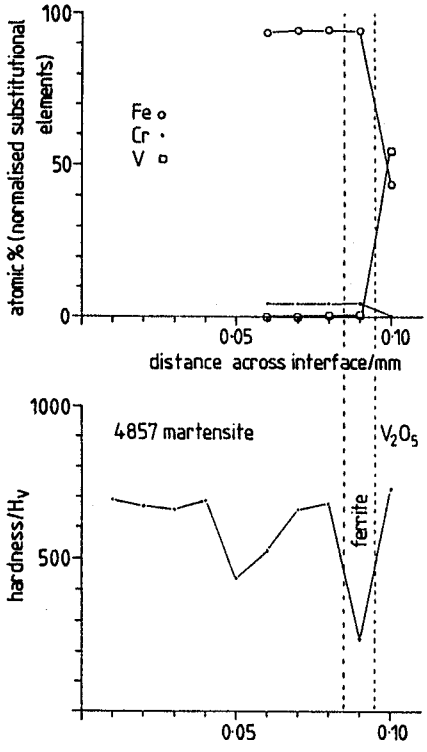

Figure 9.21. EDS trace across 4857/V_2O_5 interface after heat treatment.

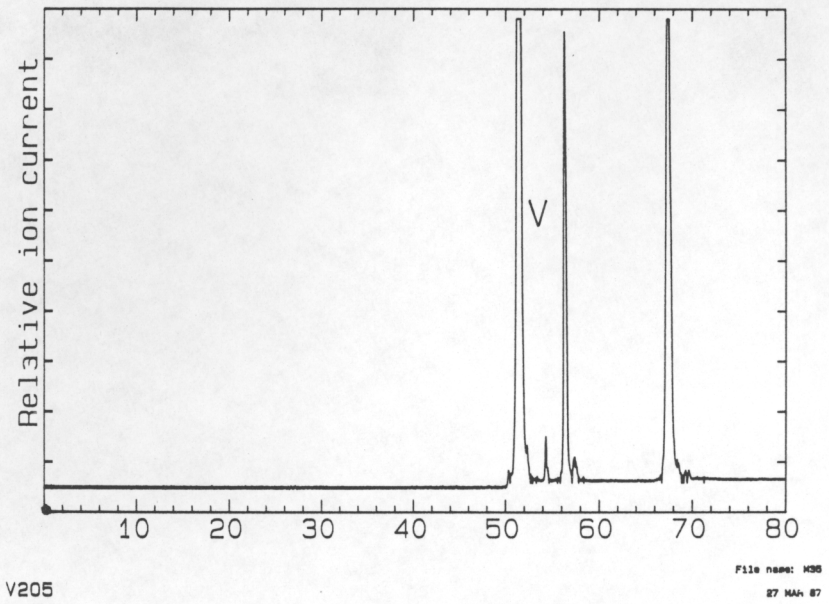

Figure 9.22. LAMMS spectrum of V_2O_5 after heat treatment.

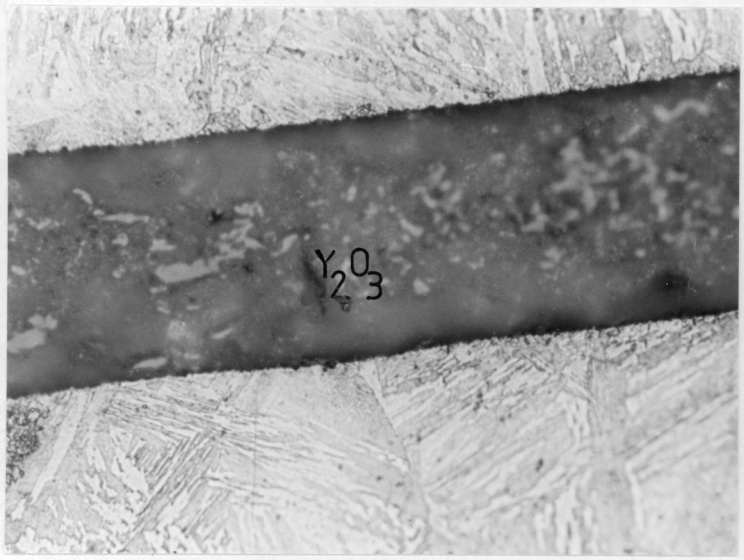

(a) 15μm

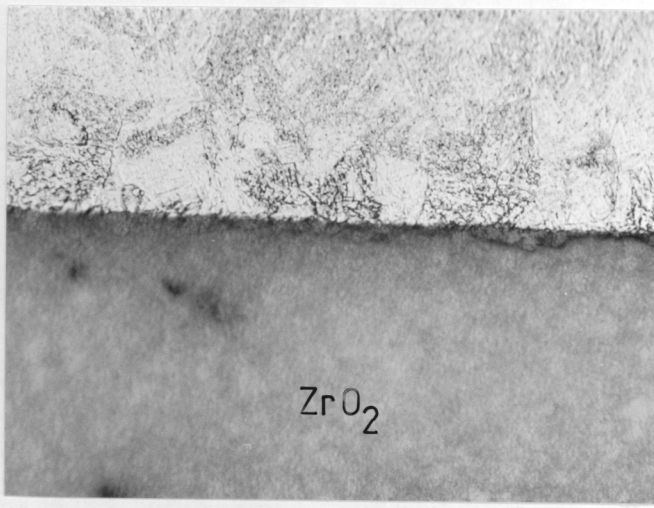

(b) 10μm

Figure 9.23. Interface regions for (a) Y_2O_3/4857,ZrO_2./ZrO_2. 900°C/10 mins - 505°C/60s. (b) 4857/ZrO_2, 900°C/10 mins-450°C/300s.

10. Conclusions and Further Work

10.1 Acicular Ferrite

The detailed analysis of Chapter 4 has revealed that acicular ferrite is a form of bainite intragranularly nucleated on deoxidation products. However, to fully describe the transformation, quantitative surface tilting values are required. These will allow the strain energy associated with the transformation to be determined and allow the governing thermodynamics to be accurately modelled.

10.2 Microphases

The importance of carbon redistribution in austenite from prior formed ferrite phases has been deduced and is shown to be strongly dependent on interface equilibrium. The effect of interfacial equilibrium is to reduce the driving force for carbon redistribution into austenite and so results in much less diffusion than predicted by the model adopted. Modelling of carbon redistribution into austenite away from the ferrite/austenite interface needs more work and evaluation.

10.3 Inclusion Nucleation Studies

A viable mechanism for nucleation of ferrite upon certain types of inclusion phases has been deduced. The most effective nucleation mechanism is of a chemical nature, i.e. inclusions that are *chemically active* are the most favourable sites. The studies presented here have revealed several types of chemical activity, fig. 10.1. The results of chapters 8 and 9 still have to be correlated with welding trials, where the presence of turbulent weldpools and higher temperatures may lead to modified effects. Initial attempts have been made in this direction by welding over a powder filled groove, fig. 10.2. Problems with this arise due to loss of powder, dissolution and redistribution of the particles; typical results are shown in fig. 10.3. This area also requires more work, especially nucleation of ferrite at lower temperatures ($\approx$ 450°C) and with lower carbon steels interfaced with TiO_2 and V_2O_5.

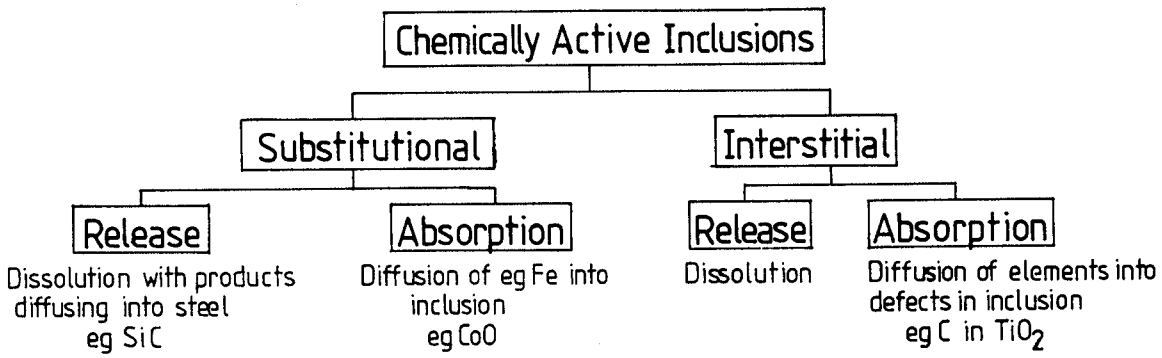

Figure 10.1.

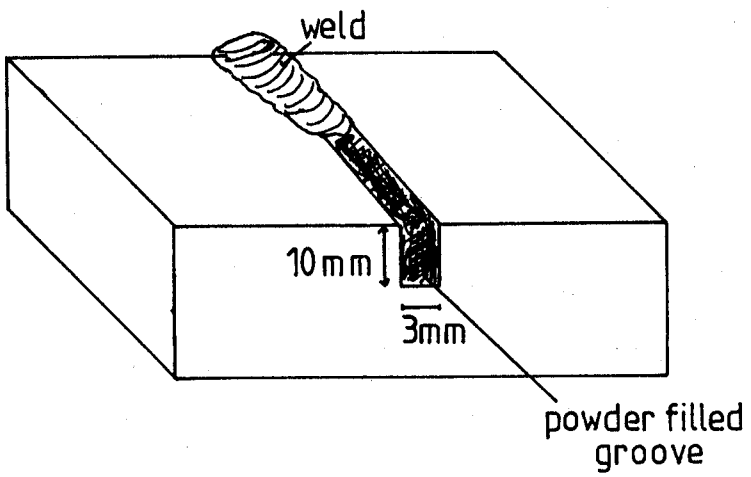

Figure 10.2.

Appendix

Matrix Notation

In order to define a vector $\underline{u}$ and relate it to other vectors, it is necessary to have a reference set of co-ordinates. For a cubic crystal, this reference set are most conveniently provided by the orthogonal axes of the unit cell, $\underline{a}_1$, $\underline{a}_2$ and $\underline{a}_3$, fig. A1. The vectors $\underline{a}_i$ are the basis vectors and the basis is A, such that when $\underline{u}$ is referred to that basis:

$$\underline{u}=u_1\underline{a}_1 + u_2\underline{a}_2 + u_3\underline{a}_3$$

$\underline{u}$ can be represented as the row vector $(u_1\ u_2\ u_3)$ or the column vector $[u_1\ u_2\ u_3]$.

These are also given, in matrix notation, as:

$$(u_1\ u_2\ u_3)=(\underline{u};A)$$
$$[u_1\ u_2\ u_3]=[A;\underline{u}]$$

referred to the basis A.

If the vector $\underline{u}$ is now referred to a second basis B, fig. A2, then A can be transformed into B by the action of a co-ordinate transformation represented by the matrix

$$(B\ J\ A)$$

So that $(\underline{a}_1\ \underline{a}_2\ \underline{a}_3)=(\underline{b}_1\ \underline{b}_2\ \underline{b}_3)(B\ J\ A)$ in this case

$$\underline{a}_1= 1\underline{b}_1 + 1\underline{b}_2 + 0\underline{b}_3$$
$$\underline{a}_2=-1\underline{b}_1 + 1\underline{b}_2 + 0\underline{b}_3$$
$$\underline{a}_3= 0\underline{b}_1 + 0\underline{b}_2 + 1\underline{b}_3$$

i.e.

$$(B\ J\ A)= \begin{matrix} 1 & 1 & 0 \\ -1 & 1 & 0 \\ 0 & 0 & 1 \end{matrix}$$

and can be used to transform $\underline{u}$ between bases A and B as

$$[B;\underline{u}]=(B\ J\ A)[A;\underline{u}]$$

As a matrix (B J A) has a transpose (A J' B) and inverse (A J B) for which

$$(\underline{u};B)=(\underline{u};A)(A\ J'\ B)$$
$$[A;\underline{u}]=(A\ J\ B)[B;\underline{u}]$$
$$(\underline{u};A)=(\underline{u};B)(B\ J'\ A)$$

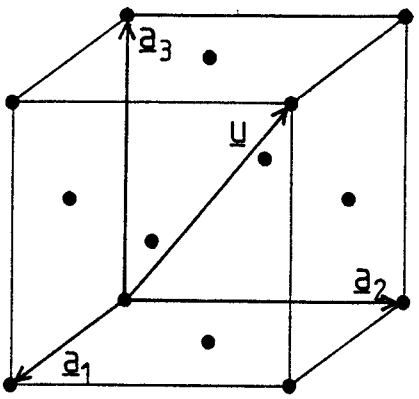

Figure A1.

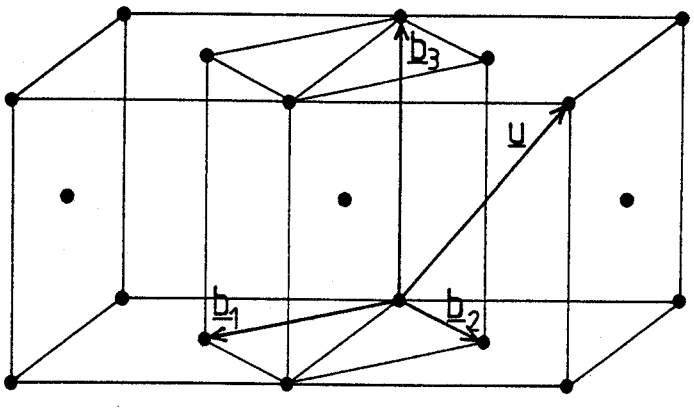

Figure A2.

References

1. T.W.Eager, *The Physics and Chemistry of Welding Processes*, Keynote Speech, International Trends in Welding Research, ASM Conference, Gatlinburg, TN., May 1986.

2. Report of Royal Commission into the Failure of King's Bridge, Melbourne, (1963).

3. W.D.Biggs, *The Brittle Fracture of Steel*, MacDonald & Evans, London, (1960).

4. R.B.Smith & R.J.Eiber, *Field Failure Survey and Investigations*, Symposium on Linepipe Research, American Gas Association, Dallas, (1969).

5. K.E.Easterling, *Introduction to the Physical Metallurgy of Welding*, Butterworths, London, (1983).

6. Alexander L.Kielland - Ulykken (Norwegian), Norges offentlige utredning Nov. 1981:11, University Press, Oslo, (1981).

7. J.V.Sharp, *J. Mat. Sci.*, 14, (1979), pp1773-1779.

8. H.K.D.H.Bhadeshia, L.-E.Svensson & B.Gretoft, *Acta Metall.*, 33, (1985), pp1271-1284.

9. G.J.Davies, *Solidification and Casting*, Applied Science, London, (1973).

10. G.J.Davies & J.G.Garland, *Int. Met. Rev.*, 20, (1975), pp83-106.

11. W.F.Savage, *Welding in the World*, 18, (1980), pp89-114.

12. W.F.Savage et al., *Weld. J.*, 44, (1965), p175.

13. W.F.Savage & A.H.Aronson, *Weld. J.*, 45, (1966), p85

14. H.Nakagawa et al., *J. Japan Weld. Soc.*, 39, (1970), p94.

15. F.Matsuda et al., *Trans. Nat. Research Inst. Metals (Japan).*, 11, (1969), p43.

16. R.S.Bray et al., *Weld. J.*, 48, (1969), p181.

17. C.R.Loper et al., *Weld. J.*, 48, (19699, p171.

18. J.C.Ion, K.E.Easterling & M.F.Ashby, *Acta Metall.*, 32, (1984), pp1949-1962.

19. W.F.Savage & E.S.Szekeres, *Weld. J.*, 46, (1967), p94.

20. D.S.Duvall & W.A.Owczarski, *Weld. J.*, 47, (1968), p115.

21. A.M.Makara & A.A.Rossoshinskii, *Automat. Weld. (USSR)*, 9, (1956), p65.

22. T.F.Chase, Jr., M.S. Thesis, Rensselaer Polytechnic Institute, Troy, N.Y., (1967).

23. H.Nakagawa et al., *Trans. Japan Weld. Soc.*, 2, (1971), p10.

24. M.Kato et al., *Trans. Japan Weld. Soc.*, 3, (1972), p59.

25. C.F.Loper & J.T.Gregory, *Proc. Spring Meeting*, 166, (1973), American Welding Society.

26. F.Matsuda et al., *Trans. Nat. Research Inst. Metals (Japan).*, 11, (1969), p43.

27. M.Kato et al., *Trans. Japan Weld. Soc.*, 3, (1972), p69.

28. T.W.Miller, M.S. Thesis, Rensselaer Polytechnic Institute, Troy, N.Y., (1967).

29. J.G.Garland, Ph.D. Thesis, University of Cambridge, (1972).

30. R.I.Southin, *Trans. AIME*, 239, (1967), p22.

31. M.C.Flemings, *Solidification Processing*, McGraw-Hill, New York, (1974).

32. J.W.Rutter & B.Chalmers, *Can. J. Phys.*, 31, (1953), p15.

33. W.A.Tiller, J.W.Rutter, K.A.Jackson & B.Chalmers, *Acta Metall.*, 1, (1953), p428.

34. H.D.Brody, *Advances in Welding Science and Technology*, ASM International, Metals Park, OH., (1987), pp83-91.

35. W.A.Tiller & J.W.Rutter, *Can. J. Phys.*, 34, (1956), p96.

36. K.E.Easterling, *Mats. Sci. & Eng.*, 65, (1984), pp191-198.

37. R.C.Cochrane & B.R.Keville, *Steels for Line Pipe and Pipeline Fittings*, Metals Society, London, (1983), pp51-60.

38. T.W.Miller, M.S. Thesis, Rensselaer Polytechnic Institute, Troy, N.Y., (1967).

39. W.F.Savage, E.F.Nippes & T.W.Miller, *Weld. J. (Res. Supplement)*, 55, (1976), pp165s-173s.

40. D.L.Cheever & D.G.Howden, *Weld. J.*, 48, (1969), p179.

41. J.G.Garland & G.J.Davies, *Met. Const.*, 2, (1970), p171.

42. F.T.Bower, H.D.Brody & M.C.Flemings, *Trans.-AIME*, 236, (1966), p624.

43. H.D.Brody & M.C.Flemings, *Trans.-AIME*, 236, (1966), p615.

44. M.C.Flemings, D.R.Poirier, V.R.Bacone & H.D.Brody, *J.I.S.I.*, 208, (1970), p371.

45. H.Fredriksson, *Metall. Trans.*, 3, (1972), p2989.

46. H.Fredriksson, *Scand. J. Metall.*, 5, (1976), p27.

47. T.Edvardsson, H.Fredriksson & I.Svensson, *Met. Sci.*, 10, (1976), pp298-306.

48. H.Fredriksson & J.Stjerndahl, *Met. Sci.*, 16, (1982), pp575-585.

49. D.A.Porter & K.E.Easterling, *Phase Transformations in Metals and Alloys*, Van Nostrand Reinhold, London, (1981).

50. B.Gretoft, H.K.D.H.Bhadeshia & L.-E.Svensson, *Acta Stereol.*, 5, (1986), pp365-371.

51. A.A.B.Sugden, unpublished research, University of Cambridge, (1986).

52. B.Gretoft, unpublished research, ESAB AB, Sweden, (1986).

53. D.J.Widgery & G.G.Saunders, *Microstructures in Steel Weld Metals*, Weld. Inst. Res. Bulletin, 16, (1975), pp277-281.

54. J.E.Indacochea & D.L.Olson, *J. Mats. Energy Systems*, 5, (1983), pp139-148.

55. D.R.Uhlmann, B.Chalmers & K.A.Jackson, *J. Appl. Phys.*, 35, (1964), pp2986-2993.

56. G.F.Bolling & J.Cisse, *J. Cryst. Growth*, 10, (1974), pp56-66, 67-76.

57. G.S.Barritte, Ph.D. Thesis, University of Cambridge, (1982).

58. M.Dadian, *Advances in Welding Science and Technology*, ASM International, Metals Park, OH., (1987), pp101-117.

59. C.A.Dube, Ph.D. Thesis, Carnegie Institute of Technology, (1948).

60. D.J.Widgery, Ph.D. Thesis, University of Cambridge, (1974).

61. R.C.Cochrane, *British Steel Research Report*, T/PDM/462/1/77/C, (1977).

62. D.J.Abson & R.E.Dolby, *Welding Institute Res. Bulletin*, 21(4), (1980).

63. Y.Ito & M.Nakanishi, *The Sumitomo Search*, no.15, (1976).

64. Committee of Weld. Metallurgy, Japan Welding Soc., *Classification of Microstructure in low C, low alloy Steel Welds Metal and Terminology*, IIW Doc. IX-1282-83, (1983).

65. R.A.Ricks, G.S.Barritte & P.R.Howell, *J. Mat. Sci.*, 17, (1982), pp732-740.

66. H.K.D.H.Bhadeshia, L.-E.Svensson & B.Gretoft, *J. Mat. Sci.*, 21, (1986), pp3947-3951.

67. M.Hillert, *Metall. Trans.*, 6A, (1975), p5.

68. J.W.Cahn, *Acta Metall.*, 8, (1960), pp554-561.

69. G.V.Shcherbedinskiy & L.A.Kondrachenko, *Phys. Metal. Metalloved*, 30, (1970), pp13-21.

70. D.E.Coates, *Metall. Trans.*, 3, (1972), pp1203-1212.

71. D.E.Coates, *Metall. Trans.*, 4, (1973), pp395-396.

72. D.E.Coates, *Metall. Trans.*, 4, (1973), pp1077-1086.

73. J.S.Kirkaldy, *Can. J. Phys.*, 36, (1958), pp907-916.

74. M.Hillert, Monograph no.33, Institute of Metals, London, (1969), p231.

75. D.E.Coates, *Metall. Trans.*, 4, (1973), pp2312-2325.

76. M.Enomoto & H.I.Aaronson, *Scripta Metall.*, 19, (1985), pp1-3.

77. K.R.Kinsman & H.I.Aaronson, *Metall. Trans.*, 4, (1973), pp959-967.

78. H.K.D.H.Bhadeshia, *Diffusional Formation of Ferrite in Iron and its Alloys*, *Progress in Material Science*, 29(4), (1985).

79. H.I.Aaronson & K.C.Russell, in *Solid-Solid Phase Transformatins*, TMS-AIME, New York, (1982), pp371-398.

80. M.Hillert in *Lectures on the Theory of Phase Transformations*, TMS-AIME, Warrendale, Pa., (1975), pp1-50.

81. H.K.D.H.Bhadeshia, *Met. Sci.*, 16, (1982), pp159-165.

82. J.S.Kirkaldy, B.A.Thomson & E.A.Baganis in *Hardenability Concepts with Applications to Steel*, TMS-AIME, Warrendale, Pa., (1978), pp82-125.

83. E.Levine & D.C.Hill, *Metall. Trans.*, 8A, (1977), pp1453- 1463.

84. R.E.Dolby, *Weld. Inst. Res. Rep.*, 14/1976/M, (1976).

85. L. Onsager, *Ann. N.Y. Acad. Sci.*, 46, (1945-6), pp241- 265.

86. J.S.Kirkaldy, *Can. J. Phys.*, 36, (1958), pp907-916.

87. L.C.Brown & J.S.Kirkaldy, *Trans. TMS-AIME*, 230, (1964), pp223-226.

88. A.Hultgren, *Trans.-AIME*, 39, (1947), pp915-1005.

89. A.Hultgren, *Jernkontorets Ann.*, 135, (1951), pp403-494.

90. C.Zener, *J. Appl. Phys.*, 20, (1949), pp950-953.

91. J.R.Bradley & H.I.Aaronson, *Metall. Trans.*, 12A, (1981), p1729.

92. F.S.Ham, *Quart. Appl. Maths.*, 17, (1959), pp137-150.

93. F.V.Nolfi, P.G.Shewmon & J.S.Foster, *TMS-AIME*, 245, (1969), p1427.

94. J.W.Christian, *The Theory of Transformatons in Metals and Alloys*, 2nd. Edition, Pt.1, Pergamon Press, Oxford, (1975).

95. J.W.Cahn & J.E.Hilliard, *J. Chem. Phys.*, 28, (1958), p258.

96. G.M.Evans, *IIW Doc II-A-546-81*, (1981).

97. D.J.Abson, *Weld. Inst. Res. Rep.*, 194, (1982).

98. G.M.Evans, *IIW Doc II-A-432-77*, (1977).

99. G.M.Evans, *Met. Const.*, 18, (1986), pp438R-444R.

100. G.M.Evans, *IIW Doc II-A-666-86*, (1986).

101. G.M.Evans, *Met. Const.*, 18, (1986), pp631R-636R.

102. G.M.Evans, *Met. Const.*, 17, (1985), pp676R-682R.

103. B.G.Kenny, H.W.Kerr, R.B.Lazor & B.Graville, *Met. Const.*, 17, (1985), pp374R-381R.

104. H.K.D.H.Bhadeshia, *Acta Metall.*, 29, (1981), pp1117- 1130.

105. R.Trivedi, *Metall. Trans.*, 1, (1970), p921.

106. R.Trivedi, *Acta Metall.*, 18, (1970), p287.

107. D.E.McRobie, Ph.D. Thesis, University of Cambridge, (1985).

108. Y.Ito, M.Nakanishi & Y-I.Komizo, *Met. Con.*, 14, (1982), pp472-478.

109. J.G.Garland & P.R.Kirkwood, *Met. Const.*, 7, (1975), pp275-283, 320-330.

110. N.Christensen & T.Simonsen, *Scand. J. Metall.*, 10, (1981), pp147-156.

111. O.Grong & D.R.Matlock, *Int. Met. Rev.*, 31, (1986), pp27- 48.

112. D.J.Abson & R.J.Pargeter, *Int. Met. Rev.*, 31, (1986), pp141-194.

113. R.A.Farrar & M.N.Watson, *Met. Const.*, 11, (1979), pp285- 286.

114. S.Nicholson & P.F.Rogers, *Welding in Offshore Constructions*, Welding Institute, Abington, (1974), pp147-166.

115. P.Judson & D.McKeown, *2nd. International Conference on Offshore Welded Structures*, Paper 3, Welding Institute, Abington, (1982).

116. A.J.Pacey, E.S.Kayali & H.W.Kerr, *Can. Metall. Q.*, 21, (1982), p309.

117. D.C.Hill & E.Levine, *Physical Metallurgy of Metal Joining*, AIME, New York, (1980), pp36-52.

118. H.Sakaki, *J. Japan Weld. Soc.*, 28, (1959), pp858-863.

119. D.J.Abson, *A Study of the Influence of C and Si on the Microstructure and Toughness of Submerged Arc Welds*, Report No. 68/1978/M, Welding Institute, Abington, (1978).

120. G.M.Evans, IIW Doc. II-A-630-84, (1984).

121. G.Snieder & H.W.Kerr, *Can. Metall. Q.*, 23, (1984), pp315-325.

122. D.W.Yu, H.S.Ann, J.H.Devletian & W.E.Wood, *Advances in Welding Science and Technology*, ASM International, Metals Park, Oh., (1987), pp267-272.

123. J.Tenkula & V.K.Heikkinen, *Weld. Res. Int.*, 8, (1978), pp369-377.

124. H.Terashima & P.H.M.Hart, *Effect of Al in C-Mn Steel on Microstructure and Toughness of SA Weld Metal - a Progress Report*, Res. Rep. 186/1982, Welding Institute, Abington, (1982).

125. H.Terashima & P.H.M.Hart, *64th. Annual AWS Convention*, Philadelphia, Pa., (1983), Paper 26C.

126. H.Terashima & P.H.M.Hart, *The Effects of Residual, Impurity and Microalloying Elements on Weldability and Weld Properties*, Welding Institute, Abington, (1984), Paper 27.

127. B.M.Kapadia in *Hardenability Concepts with Applications to Steel*, TMS-AIME, Warrendale, Pa., (1978), pp448-482.

128. Ph.Maitrepierre, D.Thiveller, J.Rofes-Vernis, D.Rousseau & R.Tricot, *ibid*, pp421-447.

129. A.H.Koukabi, T.E.North & H.B.Bell, *Met. Const.*, 11, (1979), pp639-643.

130. Y.Horii, S.Ohkita, M.Wakabayashi & M.Namura, *Development of Welding Materials for Low Temperature Service*, Nippon Steel Corporation Report, (1986).

131. G.T.Eldis & W.C.Hagel, *Hardenability Concepts with Applications to Steel*, TMS-AIME, Warrendale, Pa., (1978), pp397- 420.

132. A.D.Batte & R.W.K.Honeycombe, *J.I.S.I.*, 211, (1973), p284.

133. N.K.Ballinger & R.W.K.Honeycombe, *Metall. Trans.*, 11A, (1980), p421.

134. R.C.Cochrane & W.B.Morrison, *Met. Tech.*, 8, (1981), pp458-465.

135. J.M.Sawhill & T.Wada, *Weld. Res.*, 1, (1975), p1s.

136. N.E.Hannerz & B.M.Jonsson-Holmqvist, *Met. Const.*, 6, (1974), p64.

137. A.G.Aleksandrov et al., *Autom. Weld.*, 30, (1977), pp32- 34.

138. Teledyne Incorporated: UK Patent No. 1 297 865, (1972).

139. Nippon Steel Corporation Patent no. GB 2 015 037B, (1982).

140. A.H.Koukabi, T.E.North & H.B.Bell, *Trends in Steels and Consumables for Welding*, Welding Institute, Abington, (1979), pp281-297.

141. H.K.D.H.Bhadeshia, *Acta Metall.*, 28, (1980), pp1103-1114.

142. H.K.D.H.Bhadeshia & D.V.Edmonds, *Acta Metall.*, 28, (1980), pp1265-1273.

143. H.K.D.H.Bhadeshia, *Acta Metall.*, 29, (1981), pp1117-1130.

144. H.K.D.H.Bhadeshia & A.R.Waugh, *Acta Metall.*, 30, (1982), pp775-784.

145. Y.A.Bagaryatski, *Dokl. Akad. Nauk. SSSR*, 73, (1950), p1161.

146. D.Rosenthal & R.Schmerber, *Weld. J.*, 17, (1938), pp2-8.

147. D.Rosenthal, *Weld. J.*, 20, (1941), pp220s-234s.

148. D.Rosenthal, *Trans. AIME*, 68, (1946), pp849-866.

149. R.J.Grosh, E.A.Trabant & G.A.Hawkins, *Q. J. Appl. Maths.*, 13, (1955), pp161s-166s.

150. P.Jhaveri, W.G.Moffatt & C.M.Adams, *Weld. J.*, 41, (1962), pp12s-16s.

151. H.Ghent, C.E.Hermance, H.W.Kerr & A.N.Strong, *Proc. Int. Conf. on Arc Physics and Weldpool Behaviour*, Welding Institute, Abington, (1979), Paper 3.

152. R.Trivedi & A.R.Srinivason, *J. Heat Transfer*, 96, (1974), pp427-428.

153. J.Szekely, *Advances in Welding Science and Technology*, ASM International, Metals Park, Oh., (1987), pp3-14.

154. S.Kou & Y.H.Wang, *Weld. J.*, 63, (1986).

155. C.L.Chun, R.Zehr, J.Mazumder & M.M.Chen, *Proc. Engineering Foundatin Conf. on the Modelling and Control of Welding and Casting Processes*, Santa Barbara, Cal., (1986).

156. J.Goldak, M.McDill, A.Oddy, R.House, X.Chi & M.Bibby, *Advances in Welding Science and Technology*, ASM International, Metals Park, Oh., (1987), pp15-20.

157. P.L.Mangonon & M.A.Mahimkar, *ibid*, pp35-45.

158. J.Goldak, A.Oddy, M.McDill, A.Chakravarti, M.Bibby & R.House, *ibid*, pp523-528.

159. P.J.Alberry, *Weld. Met. Fabr.*, 49, (1981), pp543-547.

160. J.N.Clark, *Mats. Sci. & Tech.*, 1, (1985), pp1069-1080.

161. J.N.Clark, *ibid*, pp1081-1089.

162. J.N.Clark, *ibid*, pp1090-1093.

163. K.C.Russell, *Acta Metall.*, 16, (1968), p761.

164. K.C.Russell, *Acta Metall.*, 17, (1969), p1123.

165. H.K.D.H.Bhadeshia, L.-E.Svensson & B.Gretoft, *Welding Metallurgy of Structural Steels*, TMS Spring Meeting, Denver, CO., (1987).

166. R.Trivedi & G.M.Pound, *J. Appl. Phys.*, 38, (1969), p3569.

167. H.K.D.H.Bhadeshia, *Scripta Metall.*, 17, (1983), pp857-860.

168. K.J.Dalley, M.Strangwood & H.K.D.H.Bhadeshia, unpublished research, University of Cambridge, (1984).

169. D.J.Dyson & B.Holmes, *J.I.S.I.*, 208, (1970), pp469-474.

170. J.D.Watson & P.G.McDougall, *Acta Metall.*, 21, (1973), pp961-973.

171. P.L.Ryder & W.Pitsch, *Acta Metall.*, 14, (1966), p1437.

172. P.L.Ryder, W.Pitsch & R.F.Mehl, *Acta Metall.*, 15, (1967), p1431.

173. A.Crosky, P.G.McDougall & J.S.Bowles, *Acta Metall.*, 28, (1980), p1495.

174. E.S.K.Menon & H.I.Aaronson, *Acta Metall.*, 35, (1987), pp549-563.

175. D.J.Abson, *The Role of Oxygen in Controlling Weld Metal Microstructures in C-Mn Steels*, Welding Institute Res. Rep. 69/1978/M, The Welding Institute, Abington, (1978).

176. J.S.Bowles & J.K.MacKenzie, *Acta Metall.*, 2, (1954), p129.

177. M.S.Wechsler, D.S.Lieberman & T.A.Read, *Trans.- AIME*, 197, (1953), p1503.

178. H.K.D.H.Bhadeshia, *Worked Examples in the Geometry of Crystals*, Institute of Metals, London, (1987).

179. F.Ayres, *Matrices*, Schaums Outline Series, McGraw- Hill, New York, (1962).

180. W.C.Leslie, *The Physical Metallurgy of Steels*, McGraw-Hill, London, (1981).

181. J.R.Lacher, *Proc.Cambridge Philos. Soc.*, 33, (1937), p518.

182. R.H.Fowler & E.A.Guggenheim, *Statistical Thermodynamics*, Cambridge University Press, New York, (1939), p442.

183. H.K.D.H.Bhadeshia, *Met. Sci.*, 15, (1981), pp175- 177.

184. G.J.Shiflet, J.R.Bradley & H.I.Aaronson, *Metall. Trans.*, 9A, (1978), p999.

185. K.R.Kinsman & H.I.Aaronson, Discussion to J.Oblak & R.F.Hehemann, *Transformation and Hardenability in Steels*, Climax Molybdenum Co., Ann Arbor, Mich., (1967), p15.

186. H.I.Aaronson, H.A.Domian & G.M.Pound, *Trans. TMS- AIME*, 236, (1966), p768.

187. H.K.D.H.Bhadeshia, *Met. Sci.*, 15, (1981), pp178- 180.

188. H.K.D.H.Bhadeshia, *Bainite in Steels*, presented at *Phase Transformations 87*, Cambridge, (1987).

189. G.R.Shiflet, *Interface Stuctures in Pearlite, ibid.*

190. J.Crank, *The Mathematics of Diffusion*, 2nd. edition, Clarendon Press, Oxford, (1975).

191. R.M.Barrer, *Diffusion in and through Solids*, Cambridge University Press, Cambridge, (1951).

192. H.S.Carslaw & J.C.Jaeger, *Conduction of Heat in Solids*, Clarendon Press, Oxford, (1959).

193. M.H.Jacobs, *Diffusion Processes*, Springer-Verlag, Berlin, (1967).

194. W.Jost, *Diffusion in Solids, Liquids, Gases*, Academic Press, New York, (1952).

195. A.K.Shah & R.C.Sharma, *Z. Metallkde.*, 74, (1983), pp394-401.

196. L.Kaufman, S.V.Radcliffe & M.Cohen, in *Decomposition of Austenite by Diffusional Processes*, V.F.Zackay & H.I.Aaronson, eds, Interscience, New York, (1962), p313.

197. J.Crank & M.E.Henry, *Proc. Phys. Soc.*, 42B, (1949), p257.

198. G.J.Dunn, C.D.Allemand & T.W.Eagar, *Metall. Trans.*, 17A, (1986), pp1851-1863. G.J.Dunn & T.W.Eagar, *ibid*, pp1865-1871.

199. J.H.Tweed & J.F.Knott, *Met. Sci.*, 17, (1983), p45.

200. Bureau of Standards, *Chem. & Met. Eng.*, 26, (1922), p778.

201. W.Austin, *J.I.S.I.*, 92, (1915), pp157-161.

202. M.Hansen, *Constitution of Binary Alloys*, 2nd Ed., McGraw-Hill, New York, (1958).

203. O.Grong & N.Christensen, *Scand. J. Metall.*, 12, (1983), pp155-165.

204. I.Craig, T.H.North & H.B.Bell, *Trends in Steels and Consumables for Welding*, Welding Institute, Abington, (1978), Paper 21, pp249-263.

205. T.W.Eager, *Weld. J.*, 57, (1978), pp76s-80s.

206. J.H.Palm, *Weld. J.*, 51, (1972), pp358s-360s.

207. M.A.B.Noor, T.H.North & H.B.Bell, *Weld. & Met. Fab.*, 46, (1978), pp193-199.

208. T.W.Eagar in *Welding-Physical Metallurgy and Failure Phenomena*, General Electric Co., Schenectady, NY, (1979), pp31-42.

209. J.Wegrzyn, *Met. Con.*, 17, (1985), pp759R-764R.

210. N.Christensen & O.Grong, *Scand. J. Metall.*, 15, (1986), pp30-40.

211. W.P.Rees & B.E.Hopkins, *J.I.S.I.*, 172, (1952), pp403-409.

212. R.C.Cochrane & B.R.Keville in *Steels for Line Pipe and Pipeline Fittings*, The Metals Society, London, (1983), pp51- 60.

213. O.Grong, T.A.Siewart, G.P.Martins & D.L.Olson, *Metall. Trans.*, 17A. (1986), pp1797-1807.

214. F.Weinburg, *Fundamentals of Alloy Solidification Applied to Industrial Processes*, Proc. Conf., NASA, Washington DC, (1984), pp79-90.

215. C.E.Schvezov & F.Weinburg, *Metall. Trans.*, 16B, (1985), pp367-375.

216. A.A.B.Sugden & H.K.D.H.Bhadeshia, *The Non-Uniform Distribution of Inclusions in Low-Alloy Steel Weld Deposits*, accepted for publication in *Metall. Trans.*

217. D.J.Widgery, *Trends in Steels and Consumables for Welding*, The Welding Institute, Abington, (1978), pp217-229.

218. M.E.Saggese, A.R.Batti, D.N.Hawkins & J.A.Whiteman, *The Effects of Residual, Impurity and Microalloying Elements on Weldability and Weld Properties*, The Welding Institute, Abington, (1983), Paper 15.

219. A.G.Franklin, *J.I.S.I.*, 207, (1969), pp181-186.

220. R.H.Van Stone, T.B.Cox, J.R.Low Jr. & J.S.Psioda, *A Review of the Microstructural Aspects of Frcature by Dimpled Rupture*, AMAX, Ann Arbor, Mich.

221. H.C.Rogers, *Trans.-AIME*, 218, (1960), p498.

222. A.S.Argon, J.Im & A.Needleman, *Metall. Trans.*, 6A, (1975), p815.

223. A.S.Argon, J.Im & R.Safolgu, *ibid*, p825.

224. A.S.Argon & J.Im, *ibid*, p839.

225. A.S.Argon, *J. Eng. Mat. Tech.*, 98, (1976), p60.

226. L.Roesch & G.Henry, *Electron Microfractography*, ASTM STP 453, 3, (1969), Philadelphia.

227. T.B.Cox & J.R.Low Jr., *Metall. Trans.*, 5A, (1974), p1457.

228. S.Floreen & H.W.Hayden, *Scripta Metall.*, 4, (1970), p87.

229. A.H.Cottrell, in *Fracture*, Technology Press of MIT and John Wiley & Sons, New York, (1959), p20.

230. M.H.Druyresteyn, F.T.Klostermann, J.Roos, P.M.Van Dijk, P.Los & S.Radeldar, *J. Mech. Phys. Mat.*, 12, (1964), p219.

231. K.E.Puttich, *Phil. Mag.*, 4, (1959), p964.

232. A.R.Rosenfield & G.T.Hahn, *Trans.-AIME*, 59, (1966), p962.

233. M.G.Nicholas & R.M.Crispin, *J. Mat. Sci.*, 17, (1982), pp3347-3360.

234. M.F.Ashby, *Phil. Mag.*, 14, (1966), p1157.

235. L.M.Brown & J.D.Embury, *The Microstructure and Design of Alloys*, Proc. 3rd. International Conference on Strength of Metals and Alloys, Iron and Steel Institute, London,

(1975), p167.

236. F.A.McClintock, *J. Applied Mech.*, 35, (1968), p363.

237. P.Bowen, M.B.D.Ellis, M.Strangwood & J.F.Knott, ECF 6, Amsterdam, June 1986.

238. N.A.Fleck, O.Grong, G.R.Edwards & D.K.Matlock, *Weld. J. Res. Suppl.*, 65, (1986), pp113s-121s.

239. G.S.Barritte & D.V.Edmonds, *The Microstructure and Toughness of HSLA Steel Weld Metals*, Proc. Conf. on Advances in the Physical Metallurgy and Applications of Steel, The Metals Society, London, (1981), pp126-135.

240. C.S.Smith, *Trans.-AIME*, 175, (1948), p15.

241. S.Liu & D.L.Olson, *Welding Res. Suppl.*, 65, (1986), pp139s-149s.

242. D.J.Abson & R.E.Dolby, *Weld. Inst. Res. Bulletin*, 19(7), (1978).

243. R.D.Stout, P.M.Machmeir & R.Oualtroue, *Weld. J. Res. Suppl.*, 49, (1970), pp521s-530s.

244. R.C.Cochrane & P.R.Kirkwood, *Trends in Steels and Consumables for Welding*, The Welding Institute, Abington, (1978), pp103-121.

245. P.L.Harrison & R.A.Farrar, *J. Mat. Sci.*, 16, (1981), pp2218-2226.

246. D.J.Abson, R.E.Dolby & P.H.M.Hart, *Trends in Steels and Consumables for Welding*, The Welding Institute, Abington, (1978), Paper 25, pp75-101.

247. B.Ahlblom, IIW Doc. IXJ-81-84, (1984).

248. D.J.Abson, IIW Doc. IXJ-122-87, (1987).

249. J.Jang & J.E.Indacochea, *J. Mat. Sci.*, 22, (1987), pp689-700.

250. E.S.Kayali, J.M.Corbett & H.W.Kerr, *J. Mat. Sci. L.*, 2, (1983), pp123-128.

251. D.Brooksbank & K.W.Andrews, *Production and Application of Clean Steels*, Iron and Steel Institute, London, (1972), pp186-198.

252. M.Umemoto, T.Furuhara & I.Tamura. *Acta Metall.*, 34, (1986), pp2235-2245.

253. P.R.Kirkwood, *Met. Con.*, 10, (1978), pp260-264.

254. W.Cole & P.Colvin, *Met. Con. & Brit. Weld. J.*, 3, (1971), pp131-135.

255. L.M.Melnick, L.L.Lewis & B.D.Holt, *Determination of Gaseous Elements in Metals*, John Wiley & Son, New York, (1974).

256. S.Ohkita, H.Homma, T.Tsushima & N.Mori, IIW Doc. II-1070- 86, (1986).

257. T.H.North, H.B.Bell, A.Koukabi & J.Craig, *Weld. J.*, 58, (1979), pp343s-354s.

258. N.Mori, H.Homma, S.Ohkita & M.Wakabayashi, IIW Doc. IX- 1196-81, (1981).

259. J.M.Dowling, J.M.Corbett & H.W.Kerr, *Metall. Trans.*, 17A, (1986), pp1611-1623.

260. D.J.Abson, *Weld. Inst. Res. Rep.*, 69/1978/M, (1978).

261. N.Bailey & R.J.Pargeter, *Weld. Inst. Res. Rep.*, 70/1978/M, (1978).

262. L.Devillers, D.Kaplan, B.Marandet, A.Ribes & P.V.Riboud, *The Effects of Residual, Impurity and Microalloying Elements on Weldability and Weld Properties*, The Welding Institute, Abington, (1984), Paper 1.

263. R.J.Pargeter, *Weld. Inst. Res. Rep.*, 151/1981, (1981).

264. H.Homma, S.Ohkita, S.Matsuda & K.Yamamoto, *Improvement of HAZ Toughness in HSLA Steel by Finely Dispersed Ti-Oxide*, Presented at 67th AWS Convention, Atlanta, USA, (1986).

265. Y.Horii, S.Ohkita, M.Wakabayashi & M.Namura, *Development of Welding Materials for Low Temperature Service*, Nippon Steel Welding Products and Engineering Co. Ltd., Internal Report, (May 1986).

266. N.Bailey, *Weld. Inst. Res. Rep.*, 221/1983, (1983).

267. J.M.Dowling, J.M.Corbett & H.W.Kerr, *Inclusions and Residuals in Steels: Effects on Fabrication and Service Behaviour*, CANMET/CSIRA, Ottawa, (1985), pp469-486.

268. M.L.E.Davis, R.J.Pargeter & N.Bailey, *Met. Con.*, 15, (1983), pp338-344.

269. C.Bonnet & J.-P.Charpentier, *The Effects of Residual, Impurity and Microalloying Elements on Weldability and Weld Properties*, The Welding Institute, Abington, (1984), Paper 8.

270. I.Watanabe & T.Kojima, *ibid*, Paper 51.

271. R.B.Oldland, *Aust. Weld. Res.*, 14, (1985), pp44- 56.

272. G.Thewlis, Proc. Conf. *Welding and Performance of Pipelines*, The Welding Institute, Abington, (1986), Paper 9.

273. W.Shiliang, H.Weiping & T.Bogang, *Weld. Res. Int.*, 1, (1987), pp284-287.

274. B.R.Keville, *Weld. J. Res. Suppl.*, 62, (1983), pp253s-260s.

275. M.Ferrante & K.Akune, *Mat. Res. Soc. Symp.*, 21, (1984), pp817-822.

276. M.Ferrante, K.Akune & M.Odainai, *J. Mat. Sci.*, 22, (1987), pp351-355.

277. M.Strangwood & H.K.D.H.Bhadeshia, *The Welding Metallurgy of Structural Steels*, TMS-AIME Spring Meeting, Denver, CO, (1987).

278. B.Gretoft, H.K.D.H.Bhadeshia & L.-E.Svensson, Proc. of *4th. European Conference on Stereology*, pub. Chalmers University, Gothenburg, Sweden, (1985).

279. O.Kubascheswki, E.Ll.Evans & C.B.Alcock, *Metallurgical Thermochemistry*, 4th. Ed., Pergamon Press, Oxford, (1967).

280. C.H.P.Lupis, *Chemical Thermodynamics of Materials*, North Holland, Amsterdam, (1983).

281. *Phase Diagrams for Ceramists*, American Ceramic Society, Columbus, Oh, (1969-1984).

282. K.Hoshino & N.L.Peterson, *J. Phys. Chem. Solids*, 45, (1984), pp963-972.

283. M.J.Southon, M.C.Witt, A.Harris, E.R.Wallach & J.Myatt, *Vacuum*, 34, (1984), pp903-909.

284. H.Terauchi & J.B.Cohen, *J. Phys. Chem. Solids*, 39, (1978), pp681-686.

285. S.P.Denker, *J. Less-Common Metals*, 14, (1968), p1.

286. A.S.Boruckovich, *Phys. Status Solidi*, A46, (1978), p11.

287. J.Calais, *Adv. Phys.*, 26, (1977), p847.

288. J.M.Schoen, *Phys Rev.*, 184, (1969), p858.

289. J.M.Schoen & S.P.Denker, *Phys Rev.*, 184, (1969), p864.

290. A.L.Ivanovsky, V.A.Gubanov, G.P.Schveikin & E.Z.Kumarev, *J. Less-Commmon Metals*, 78, (1981), p1.

291. V.A.Gubanov, A.L.Ivanovsky, G.P.Schveikin & D.E.Ellis, *J. Phys. Chem. Solids*, 45, (1984), pp719-730.

292. D.Watanabe, O.Terasaki, A.Jostsons & J.R.Castles, in *The Chemistry of Extended Defects in Non-Metallic Solids*, L.Eyring & M.O'Keeffe (Eds), North Holland, Amsterdam, (1970), pp238-258.

293. A.Magnéli, *ibid*, pp148-163.

294. L.A.Bursill & B.G.Hyde, *Phil. Mag.*, 23, (1971), p3.

295. B.G.Hyde & L.A.Bursill, in *The Chemistry of Extended Defects in Non-Metallic Solids*, L.Eyring & M.O'Keeffe (Eds), North Holland, Amsterdam, (1970), pp347-378.

296. P.Kofstad, *J. Phys. Chem. Solids*, 23, (1962), p1579.

297. K.S.Forland, *Acad. Chem. Scand.*, 18, (1964), p1267.

298. C.Picard & P.Gerdanian, *J. Solid State Chem.*, 14, (1975), p66.

299. R.-T.Dirstine & C.J.Rosa, *Z. Metallkde*, 70, (1979), p322.

300. C.B.Alcock, S.Zador & B.C.H.Steele, *Electromotive Force Measurements in High Temperature Systems*, Institute of Mining and Metallurgy, London, (1968).

301. J.-F.Marucco, J.Gautron & P.LeMasson, *J. Phys. Chem. Solids*, 42, (1981), pp363-367.

302. S.Zador in *Electromotive Force Measurements in High Temperature Systems*, Institute of Mining and Metallurgy, London, (1968).

303. G. Dearnaley, A.M. Stoneham & D.V. Morgan, "Reports on Progress in Physics", 33, (1970), p 1129.

304. M.D.Bui, C.Jardin, J.P.Gauthier, G.Thollet & P.Michel, *Titanium 80, Science and Technology*, TMS-AIME, Warrendale, Pa, (1980), pp2819-2827.

305. A.R.Mills, G.Thewlis & J.A.Whiteman, *The Nature of Inclusions in Steel Weld Metals and their Influence on the Formation of Acicular Ferrite*, to be published, *Mat. Sci. & Tech.*, Nov/Dec. 1987.